REACTIVITY OF TRIVALENT METALS TOWARDS THE KEGGIN-TYPE [SbW₉O₃₃]⁹⁻ TRILACUNARY POLYOXOANION

Author:

CARLOS ASENSIO REGALADO

Supervisors:

BEÑAT ARTETXE ARRETXE

SANTIAGO REINOSO CRESPO

Leioa, 28 June 2016

TRABAJO FIN DE GRADO
GRADO EN QUÍMICA

REACTIVITY OF TRIVALENT METALS TOWARDS THE KEGGIN-TYPE [SbW$_9$O$_{33}$]$^{9-}$ TRILACUNARY POLYOXOANION

MEMORIA PRESENTADA POR CARLOS ASENSIO REGALADO

FECHA DE MATRICULACIÓN Y DEFENSA: JUNIO-JULIO 2016

DIRECTORES: BEÑAT ARTETXE ARRETXE
SANTIAGO REINOSO CRESPO

DEPARTAMENTO: QUÍMICA INORGÁNICA

TABLE OF CONTENTS

1. INTRODUCTION

Polyoxometalates (POMs) are a well-known family of anionic metal-oxygen clusters with unique electronic versatility and structural diversity. These features make POMs remarkable compounds with a wide range of applications in fields like catalysis, materials science or biomedicine, and they continue to attract increasing attention worldwide.[1] J. J. Berzelius is thought to be the first scientist to synthesize a polyoxometalate back in 1826, namely the ammonium salt of the $[PMo_{12}O_{40}]^{3-}$ anion.[2] However, the Elhuyar brothers had already prepared a POM almost 40 years before (1783), describing it as a bitter, spicy, yellow salt containing tungsten.[3] The first structural evidence of a POM cluster was the determination of the crystal structure of the $H_3[PMo_{12}O_{40}]$ acid by J. F. Keggin using powder X-ray diffraction.[4] Since then, POM chemistry has expanded very quickly in the last decades on the basis of Pope's seminal work dating back to the 80's,[5,6] and it can be considered as one of the most dynamic fields of the inorganic chemistry at present.[7]
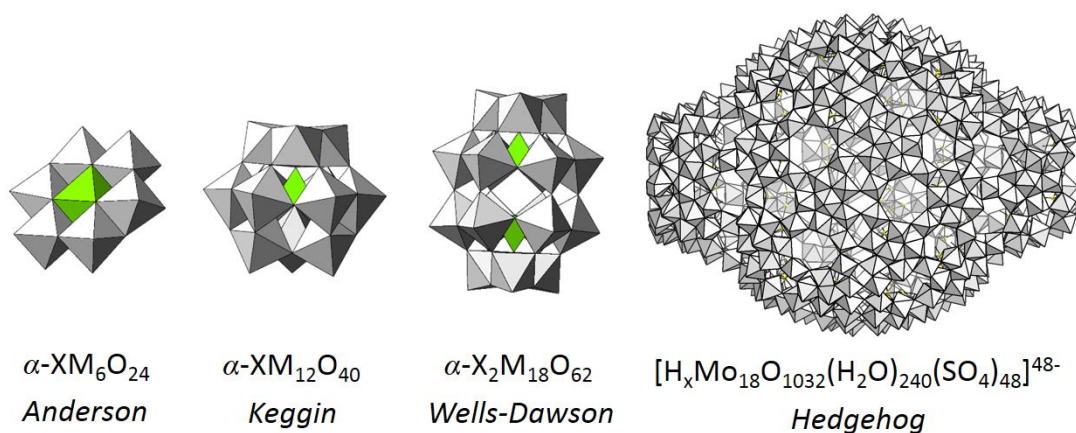

α-XM_6O_{24}
Anderson

α-$XM_{12}O_{40}$
Keggin

α-$X_2M_{18}O_{62}$
Wells-Dawson

$[H_xMo_{18}O_{1032}(H_2O)_{240}(SO_4)_{48}]^{48-}$
Hedgehog

Figure 1.- Structural diversity in POMs. Examples of the most representative hetero-POMs. Colour code: $\{MO_x\}$, grey polyhedra; $\{XO_n\}$, green polyhedra.

The great range of approaches for the preparation of this kind of anions has resulted in a huge variety of structures, comprising from small and simple anions to complex clusters showing sizes comparable to those of proteins (Figure 1). POMs are composed of early transition metals (known as *addenda atoms*) from groups 5 and 6, usually in their highest oxidation states. Traditionally, V, Mo or W, but also Nb or Ta

can act as addenda metal centres.[8] These metals show a suitable combination of charge and ionic radius, as well as empty and accessible d orbitals available for electronic back-donation in the formation of π M–O bonds.

The protonation of an oxometallate ion under particular conditions gives rise to polycondensation of {MO$_x$} units and formation of more complex structures called polyanions. Structurally, POMs are formed by the condensation of polyhedral {MO$_x$} units, where the coordination numbers of the metallic centres are between 4 and 7, and the octahedral (6) is the most common geometry. The {MO$_6$} units can condense sharing vertices or edges (exceptionally faces) (Figure 2), in such a way that a maximum of two oxygen atoms per octahedron can be left unshared (Lipscomb's principle)[9], which minimizes the strong *trans*-effect of the terminal M–O bonds and avoids the dissociation of the cluster. This oligomerization is not infinite; due to the polarization of the peripheral addenda metal centres toward the outer oxygen shell, vacant and accessible d orbitals of the metal allow for the formation of terminal M=O double bonds, preventing the subsequent formation of bridges with additional octahedra.
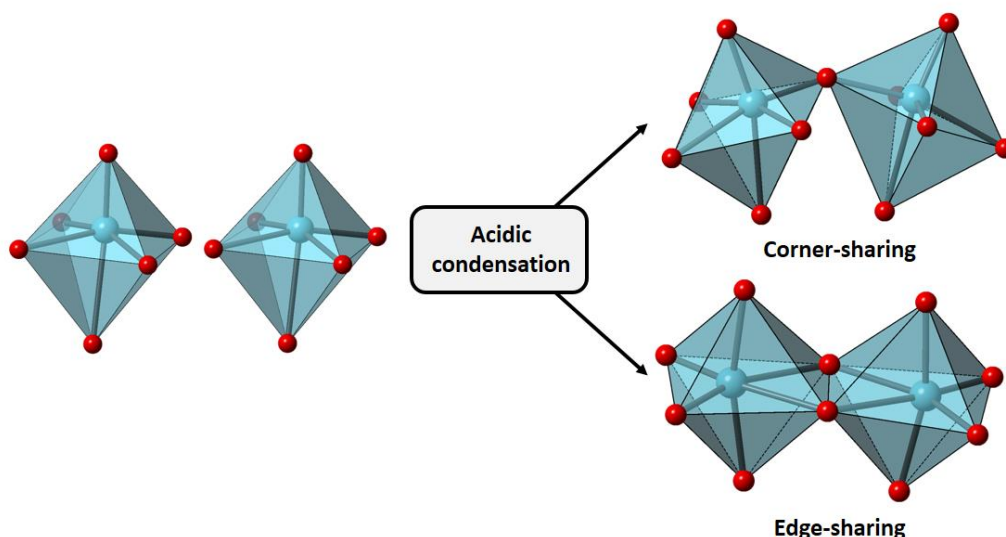

Figure 2.- Schematic representation of the two common linkage modes between octahedral {MO$_6$} units: corner-sharing (top right) and edge-sharing (bottom right).

Despite the wide variety of structures, most POMs exhibit some common features:[10]

(a) POMs usually show high charge, size and symmetry, as well as thermal and solution stability.

(b) The formation equilibria of POMs is highly dependent on the concentration of the reactants, pH, ionic strength, presence of extra ligands, counterions employed, temperature or pressure. It is usual that different POM species coexist in solution at a given pH value.

(c) Species containing alkaline counterions are usually water soluble, whereas organic counterions confer high solubility in organic solvents on the polyanions.

(d) POMs can be used as inorganic ligands due to their ability to coordinate cations, anions or neutral molecules with the oxygen atoms located at the surface.

1.1. CLASSIFICATION

Depending on their composition, POMs can be classified into two main groups:

Isopolyoxometalates (iso-POMs), of general formula $[M_mO_y]^{q-}$, are exclusively constituted by early transition metals and oxygen. The structures of most iso-POMs are derived from the $[M_{10}O_{28}]^{q-}$ decametalate anion *via* elimination of octahedral units. Examples of the most common species include the β-M_8O_{26} octametalate, M_7O_{24} heptametalate (parametalate-A) and the M_6O_{19} hexametalate (Lindqvist-type) anions (Figure 3). Furthermore, some other iso-POM whose structures are not directly derived from the decametalate cluster include the $\{W_{12}O_{40}(OH)_2\}^{10-}$ anion (paratungstate-B).
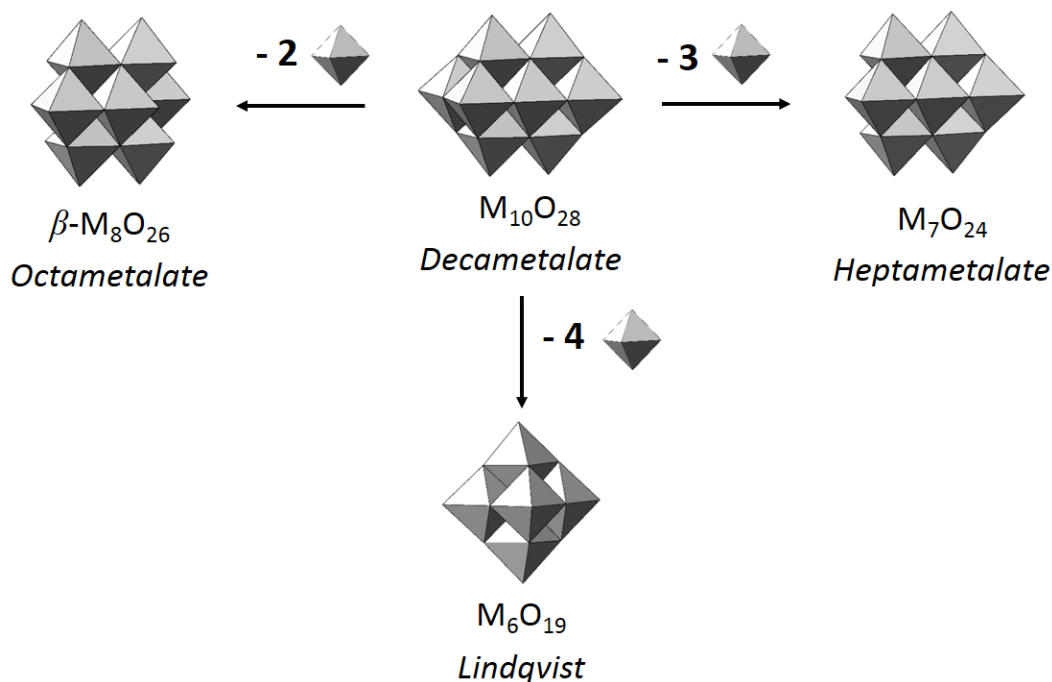
Figure 3.- Structures of the most common iso-POMs derived from the $[M_{10}O_{28}]^{q-}$ decametalate by removal of $\{MO_6\}$ octahedra.

Heteropolyoxometalates (hetero-POMs), of general formula $[X_xM_mO_y]^{q-}$ contain additional elements known as heteroatoms (X) besides metal and oxygen. The nature of X does not show any specific restriction, as many of the elements of the periodic table, with the exception of noble gases, are known to be able to act as heteroatoms. Heteropolyoxotungstates are the most studied POMs and illustrative examples include the $[XW_6O_{24}]^{n-}$ Anderson-Evans anion, which contains an octahedral heteroatom (X = first-row transition metals, Al^{III}, Ga^{III}, ...); the Keggin anion $[XW_{12}O_{40}]^{n-}$, which contains a tetrahedral heterogroup (usually X = B^{III}, Si^{IV}, Ge^{IV}, P^{V}, As^{V}); and the Wells-Dawson anion $[X_2W_{18}O_{62}]^{n-}$ derived from the Keggin structure and showing two tetrahedral heteroatoms (X = typically from group 15). The molecular structures of these hetero-POMs have already been shown in Figure 1.

1.2. THE KEGGIN ANION

Acidic condensation of $\{MO_6\}$ units in the presence of tetrahedral $[XO_4]^{n-}$ oxoanions usually results in α-$XM_{12}O_{40}$ Keggin-type structures. The Keggin anion is constituted by four $\{M_3O_{13}\}$ trimers formed by three edge-sharing $\{MO_6\}$ octahedra. These trimers are linked to each other and to the central tetrahedron through corner-sharing in an ideal tetrahedral (T_d) symmetry.

Keggin-type heteropolyanions have five structural isomers, known as Baker-Figgis isomers (Figure 4).[11] These isomers result from the 60° rotation of one (β), two (γ), three (δ) or four (ε) $\{M_3O_{13}\}$ trimers from the parent α-Keggin anion. The α and β isomers are the most stable, because they do not show any edge-sharing linkages between different $\{M_3O_{13}\}$ trimers. However, not only the α and β, but also the γ isomer of Keggin-type tungstosilicates and germinates can be readily isolated and have been successfully characterised both in solution and in the solid state.

α $\qquad$ β $\qquad$ γ $\qquad$ δ $\qquad$ ε
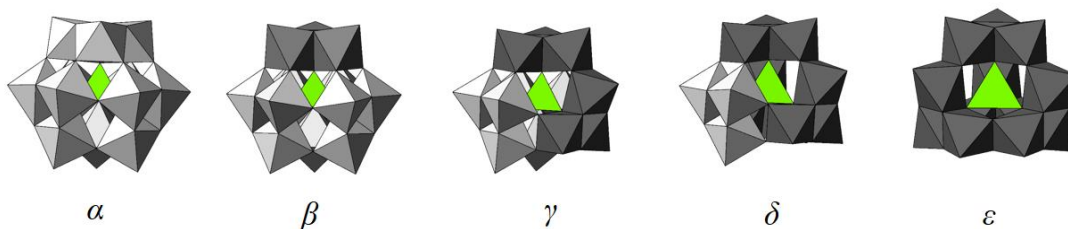
Figure 4.- Baker-Figgis isomers of the Keggin-type $\{XM_{12}O_{40}\}$ structure. Rotated trimers are shown in dark grey.

The less stable δ-Keggin-type structure has only been observed for the $[AlO_4Al_{12}(OH)_{24}(H_2O)_{12}]^{7+}$ cationic cluster,[12] whereas the lanthanide stabilized phosphomolybdates $[\varepsilon\text{-}PMo_{12}O_{36}(OH)_4\{Ln(H_2O)_4\}]^{4+}$ (Ln = La to Sm)[13] represent the only structurally characterised examples of the ε-isomer isolated as independent cluster.

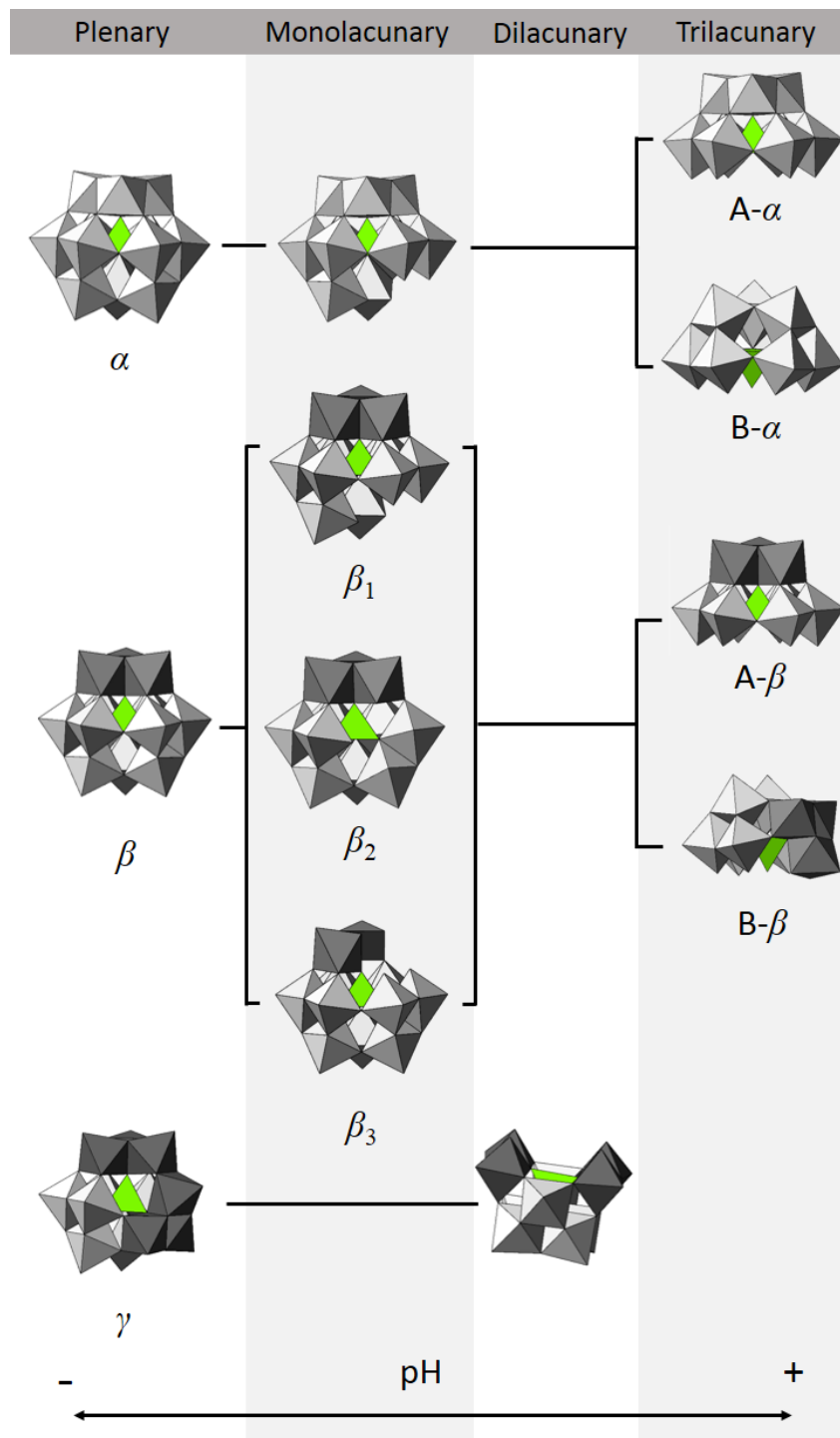*Figure 5.- Different lacunary species derived from the plenary Keggin anion and its isomers.*

Some POM structures are derived from larger parent clusters by removing one or more addenda metal atoms from the shell, resulting in defective structures known as *lacunary species*. Nine lacunary species can be obtained by removing one or more

octahedra from the parent plenary $XM_{12}O_{40}$ Keggin anion (Figure 5). From the α-isomer, mono- ($XM_{11}O_{39}$) and trivacant species (XM_9O_{34}) can be generated upon elimination of one or three octahedra, respectively. The α-XM_9O_{34} anions show two different isomers named as A or B depending on whether the eliminated $\{MO_6\}$ octahedra belong to a $\{M_3O_{15}\}$ corner-sharing triad or to a $\{M_3O_{13}\}$ edge-sharing trimer. Similar species can be isolated from the β-isomer. The lower symmetry of the β-$\{XM_{12}O_{40}\}$ cluster allows for three different monolacunary species to be formed depending on the position of the vacant site. The vacant position in the β_1-monolacunary species is located in the triad opposite to the 60°-rotated trimer, whereas it lays at the central belt and the rotated trimer for the β_2 and the β_3 forms, respectively. Up to now, only the dilacunary $XM_{10}O_{36}$ species has been isolated from the γ isomer. This dilacunary species can be generated upon elimination of the two edge-sharing octahedra belonging to different trimers.

For some specific heteroatoms like As^{III}, Sb^{III}, Te^{IV} or Se^{IV}, the presence of a lone electron pair prevents the closure of a complete Keggin shell, so that only B-XM_9O_{33} trivacant species can be formed.[14] In this type of trivacant species, the central heteroatom (X) is in a trigonal pyramidal environment with the lone electron pair pointing towards the centre of the removed trimer.
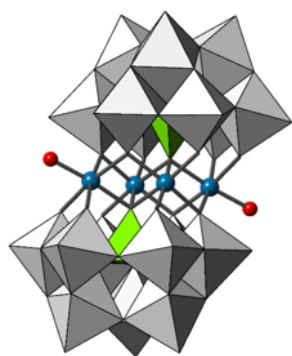
1.3. SANDWICH-TYPE POMs

Lacunary polyanions can act as multidentate ligands toward different electrophiles (e.g. p-block organoderivatives, organometallic groups, 3d- and 4f-metals) through the oxygen atoms delimiting the vacant sites. Incorporation of electrophiles in these sites to regenerate the parent cluster results in *substituted species*. The use of lacunary polyoxotungstates in combination with 3d-metals has resulted in a huge variety of substituted species with various shapes and nuclearities that exhibit interesting electrochemical, catalytic and magnetic properties.[15] In some particular cases, two Keggin-type trilacunary species can enclose additional metal centres, leading to sandwich-type POMs.[16]

Sandwich-type POMs can be classified according to the presence or absence of a lone electron pair in the heteroatom:

A) If the central heteroatom exhibits no lone pair ($[XW_9O_{34}]^{n-}$ where X = Si^{IV}, Ge^{IV}, P^V, As^V, etc.) two different kinds of sandwich-type POMs can be obtained, depending on the nature of the trilacunary unit. For the B species, anions of the formula $[M_4(H_2O)_2(B\text{-}\alpha\text{-}XW_9O_{34})_2]^{n-}$ (Weakley-type) are formed (Figure 6a). These anions can be regarded as consisting of two plenary $\{XW_9M_3\}$ substituted units with two M atoms in common.[17] The four 3d-metal centres are connected to each other through oxo-bridges resulting in a central romblike core with a total number of two terminal water molecules.

If the trilacunary Keggin units are A-type instead of B, anions of the formula $[(M(H_2O)_2)_3(A\text{-}XW_9O_{34})_2]^{n-}$ (Knoth-type) are formed (Figure 6b). In these sandwich-type POMs, the three octahedral belt metal ions are not linked to each other *via* oxo bridges, in such a way that they show two coordination water molecules each, leading to a central pocket that can host small species like CO_3^{2-} or NO_3^-.[18]

(a) $\{M_4(H_2O)_2(B\text{-}\alpha\text{-}XW_9O_{34})_2\}$
Weakley
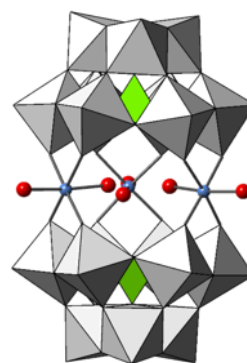
(b) $\{(M(H_2O)_2)_3(A\text{-}\alpha\text{-}XW_9O_{34})_2\}$
Knoth

Figure 6.- Examples of sandwich-type POMs that contain heteroatoms without lone electron pair; colour code: grey octahedra, $\{WO_6\}$; green tetrahedra, $\{XO_4\}$; blue, M; red, O.

B) If the central heteroatom X exhibits a lone-pair ($[XW_9O_{33}]^{n-}$ where X = As^{III}, Sb^{III}, Bi^{III}, Te^{IV}, etc.), only B-type trilacunary species can be formed, as has been previously mentioned. Within this group, two different sandwich-type POMs can be distinguished, depending on the Baker-Figgis isomer of the Keggin unit: α or β.

On the one hand, polyoxoanions with general formula $[(M(H_2O))_3(B\text{-}\alpha\text{-}XW_9O_{33})_2]^{n-}$ (Hervé-type) are formed from the $B\text{-}\alpha\text{-}XW_9O_{33}$ ($B\text{-}\alpha\text{-}XW_9$) trilacunary unit (Figure 7a). The first example of this type of POMs, the $[(Cu(H_2O))_3(B\text{-}\alpha\text{-}AsW_9O_{33})_2]^{12-}$ anion, was reported by Hervé.[19] In this cluster, the two $B\text{-}\alpha\text{-}AsW_9$ moieties are linked by three square pyramidal copper(II) cations located at belt positions. Up to six belt positions are available in this type of assembly for the coordination of metal centres, which are usually completed by the coordination of alkaline cations. Therefore, partial (di-, tri- and tetra-)[20,21] and full (hexa-)[22] substitution of these positions has been reported, especially for X = As^{III}, Sb^{III} and M = Cu^{II}. Compositional variations for the trisubstituted species include different divalent first row transition metals for X = As^{III}, Sb^{III} and Cu^{II} derivatives for X = Se^{IV}, Te^{IV}.[23] Additionally, mixed valence V^{IV}/V^V species, and palladium-substituted clusters displaying Pd^{II} centres in square-planar geometry have also been reported.[24,25] In contrast, there is only one example of a trivalent metal-substituted Hervé-type POM reported so far, namely $[(Mn^{III}(H_2O))_3((SbW_9O_{33})_2)]^{9-}$.[26] Hervé-type POMs have been studied as homogeneous catalysts for the epoxidation of dienes,[20] some members of this family have shown interesting magnetic properties,[27] and examples exhibiting interesting biomedical applications that include anti-tumor, -viral and -bacterial activities, have also been reported.[28]

On the other hand, the trilacunary {$B\text{-}\beta\text{-}XW_9$} Keggin subunits could easily assemble into sandwich-type compounds with the formula $[\{WO_2(OH)_2\}(WO_2)_2(B\text{-}\beta\text{-}XW_9O_{33})_2]^{n-}$ (Krebs-type). In these clusters, the two trilacunary subunits are linked by two inner cis-{WO_2} and two outer fac-{$WO_2(OH)$} octahedral groups in belt positions, in such a way that there is no direct connection between these belt metal centres. As indicated by Krebs and co-workers,[14] the latter groups are labile allowing defective intermediates to be formed in solution and stabilized by the incorporation of different electrophiles at the vacant external positions. Exchange of the outer

{WO$_2$(OH)} groups for {M(H$_2$O)$_3$} moieties has been thoroughly studied, resulting in a large family of 3d-metal-disubstituted [{M(H$_2$O)$_3$}$_2$(WO$_2$)$_2$(XW$_9$O$_{33}$)$_2$]$^{n-}$ Krebs-type species for M = Mn^{II}, Fe^{III}, Co^{II}, Ni^{II}, or Zn^{II} and X = Sb^{III} or Bi^{III} (Figure 7b).[29,30] Moreover, the inner positions have also been fully or partially exchanged for {M(H$_2$O)$_2$} groups in several tri- and tetrasubstituted analogues, especially for certain heteroatoms (X = Te^{IV}, Se^{IV}) or trivalent metals (M = Fe^{III}, Cr^{III}, Al^{III}, In^{III}).[29,30]

(a) {(M(H$_2$O))$_3$(B-α-XW$_9$O$_{33}$)$_2$}
Hervé

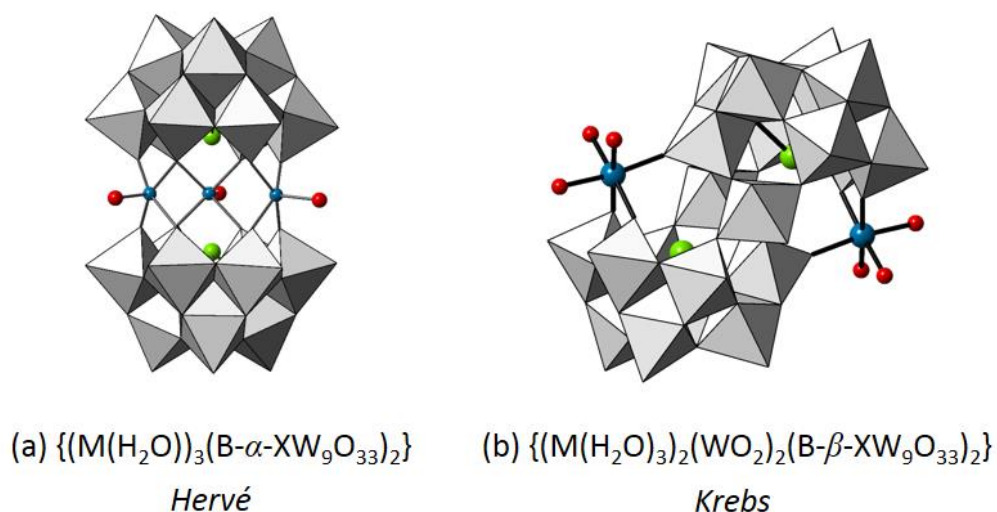(b) {(M(H$_2$O)$_3$)$_2$(WO$_2$)$_2$(B-β-XW$_9$O$_{33}$)$_2$}
Krebs

Figure 7.- Examples of sandwich-type POMs in which the heteroatom X has a lone electron pair. Colour code: same as Figure 6, but for X, green.

Due to their interesting catalytic properties, Krebs-like clusters have been incorporated into functional materials like polypyrrole films *via* POM immobilization.[31] Highly efficient catalytic activity has been observed for Krebs-type POMs in the oxygenation of cyclohexane among others.[32] Furthermore, the [Al$_4$(H$_2$O)$_{10}$(X^{III}W$_9$O$_{33}$)$_2$]$^{6-}$ species (X = As, Sb) has been employed as Lewis acid catalyst in H$_2$O$_2$-based oxidations.[20,33]

1.4. OBJECTIVE

This project has been carried out within the 'POM laboratory' research group at Departamento de Química Inorgánica, Facultad de Ciencia y Tecnología, University of the Basque Country, UPV/EHU. One of the most representative research lines in the group is based on the synthesis and characterisation of 3d- and/or 4f-metal substituted POMs.[34-37] Metal-containing species constitute one of the largest and currently most active groups within the POM chemistry because combination of POM building blocks with 3d- and/or 4f-metals has been shown to be a powerful tool for designing new architectures and introducing additional functionalities to the system, like photoluminescent, magnetic and catalytic properties.

The main objective of this work consists on **the evaluation of the reactivity of different trivalent metals** (M^{III} = Fe, Sc, Cr, Mn, Co, Al, Ga) **towards the Keggin-type [B-α-SbW$_9$O$_{33}$]$^{9-}$ trilacunary polyoxoanion**. The interest of this study resides in the fact that the reactivity of these metals has been much less studied in comparison with that of divalent metals. Although tens of examples of divalent metal-containing sandwich-type POMs can be found in the literature, trivalent metal substituted sandwich-type POMs are limited to Fe, Cr and Al derivatives of the Krebs-type POM and a single Mn-containing Hervé-type cluster.

Different compounds have been isolated in the course of these studies. Therefore, the aims of this work also include **the identification of the obtained POMs** *via* FT-IR spectroscopy, as well as **the full chemical** (elemental and thermal analyses) **and structural characterisation** (*via* single-crystal X-ray diffraction) **of those clusters with novel features**. These include compounds Na$_{12}$[{Fe(C$_2$H$_3$O$_2$)}$_3$(SbW$_9$O$_{33}$)$_2$]·36H$_2$O (**1-Fe**), Na$_{10}$[{Sc(H$_2$O)$_3$}{WO$_2$(OH)}(WO$_2$)$_2$(SbW$_9$O$_{33}$)$_2$]·43H$_2$O (**2-Sc**), and Na$_{10}$[{Mn(H$_2$O)$_3$}$_2$(WO$_2$)$_2$(SbW$_9$O$_{33}$)$_2$]·40H$_2$O (**2-Mn**). Additionally, preliminary experiments have been carried out *via* Electron Paramagnetic Resonance spectroscopic experiments have also been carried out **to get insight about more sophisticated characterisation techniques**.

As for the academic aims, they include (i) **the use of scientific databases** (crystallographic, ICSD; references, SciFinder), (ii) **comprehensive reading** of publications, (iii) the development of skills for the **writing of scientific papers** and (iv) **teamwork in a research laboratory**.

2. EXPERIMENTAL SECTION

2.1. SYNTHESIS

2.1.1. Preparation of the starting material

The $[B\text{-}\alpha\text{-}SbW_9O_{33}]^{9-}$ POM precursor was synthesized according to reported procedures[14] and identified by FT-IR spectroscopy. All other reagents were purchased from commercial sources and used without further purification.

$Na_9[B\text{-}\alpha\text{-}SbW_9O_{33}]\cdot 20H_2O$ (B-α-SbW$_9$): Sb_2O_3 (1.96 g, 6.72 mmol) suspended in concentrated HCl (10 mL) was added dropwise to a solution of $Na_2WO_4\cdot 2H_2O$ (40 g, 121.27 mmol) in water (80 mL) at 90 °C. The resulting mixture was refluxed for 1h, cooled to room temperature, filtered and left to evaporate. Crystals started forming immediately and were kept in their mother liquors for 5 days. Yield: 27 g, 63% based on W. IR (KBr): $\bar{\nu}$ (cm^{-1}): 926 (s), 891 (s), 768 (s), 706 (s), 513 (w), 467 (w), 432 (w).

2.1.2. General synthetic procedure

To a warm (40 °C) solution of $Na_9[SbW_9O_{33}]\cdot 20H_2O$ (3 g, 1 mmol) in aqueous 1 mol·L^{-1} acetic acid/sodium acetate buffer (30 mL) the corresponding trivalent metal source (1.53 mmol; $FeCl_3\cdot 6H_2O$, 414 mg; Sc_2O_3, 211 mg; $Cr(NO_3)_3\cdot 9H_2O$, 612 mg; $Mn(C_5H_7O_2)_3$, 539 mg; $Al(NO_3)_3\cdot 9H_2O$, 574 mg; $Co(C_5H_7O_2)_3$, 545 mg; or $Ga(NO_3)_3\cdot H_2O$, 419 mg) was added. The resulting mixture was stirred for 90 min at 40 °C, cooled to room temperature, filtered and left to evaporate in an open container to afford single crystals of compounds **1-Fe** and **2-M** (M = Sc, Mn) suitable for X-ray diffraction.

$Na_{12}[\{Fe(C_2H_3O_2)\}_3(SbW_9O_{33})_2]\cdot 36H_2O$ (1-Fe): big, brown plates were obtained after ca. 20 days (yield 1.89 g, 64% based on W). Anal. Calcd (found): C, 1.39 (1.35); H, 1.38

(1.32). IR (KBr): $\bar{\nu}$ (cm^{-1}): 1377 (m), 1317 (m), 949 (s), 868 (s), 737 (s), 689 (s), 521 (w), 473 (w).

Na$_{10}$[{Sc(H$_2$O)$_3$}{WO$_2$(OH)}(WO$_2$)$_2$(SbW$_9$O$_{33}$)$_2$]·47H$_2$O (2-Sc): colourless needles were obtained after ca. 5 days (yield 1.83 g, 67% based on W). IR (KBr): $\bar{\nu}$ (cm^{-1}): 957 (s), 841 (s), 804 (s), 758 (s), 665 (s), 650 (s), 610 (s), 474 (w).

Na$_{10}$[{Mn(H$_2$O)$_3$}$_2$(WO$_2$)$_2$(SbW$_9$O$_{33}$)$_2$]·35H$_2$O (2-Mn): orange plates were obtained after ca. 2 days (yield 1.11 g, 40% based on W). IR (KBr): $\bar{\nu}$ (cm^{-1}): 949 (s), 833 (s), 770 (s), 671 (m), 523 (w), 461 (w).

2.2. MATERIALS AND METHODS

The experimental techniques employed for the characterisation of compounds **1-Fe** and **2-M** (M = Sc, Mn) are described in this section.

2.2.1. Fourier transform-infrared spectroscopy (FT-IR)

The FT-IR spectra were recorded in a Shimadzu FT-IR 4800S spectrophotometer, and the data were manipulated with the IRSolutions software. All the measurements were carried out using a 4 cm^{-1} resolution in the 400-4000 cm^{-1} spectral range. The samples were prepared as pressed KBr pellets. The intensity of the signals has been described as strong (s), medium (m), and weak (w).

2.2.2. Thermogravimetry (TG)

Thermal analyses were carried out on a Mettler Toledo TGA/SDTA851^e thermobalance under a 50 cm^3 min^{-1} flow of synthetic air from room temperature to 800 °C at a heating rate of 5 °C min^{-1}.

2.2.3. Single-crystal X-ray diffraction (XRD)

The single-crystal X-ray diffraction experiments were carried out at the X-ray Service: Molecules and Materials from SGIker, University of the Basque Country UPV/EHU. Intensity data were collected at 100(2) K on an Agilent SuperNova diffractometer with monochromatized Mo Kα radiation (λ = 0.71073 Å) and Eos CCD detector for **1-**

13

Fe and **2-Mn**, and at 150(2) K with monochromatized Cu Kα radiation (λ = 1.54184 Å) and Atlas CCD detector for **2-Sc**. Data collections, unit cell determinations, intensity data integrations, and absorption corrections with face indexing were performed using the CrysAlis Pro software package.[38] The structures were solved using OLEX2-v1.2 software[39] and refined by full-matrix least-squares using SHELXL-97.[40] Thermal vibrations were treated anisotropically for heavy atoms (W, Sb, trivalent metals). For **1-Fe**, hydrogen atoms on the acetate ligands were placed in calculated positions and refined with a riding model using standard SHELXL parameters. Geometrical calculations were carried out using Platon software.[41]

For **2-Sc** and **2-Mn**, tungsten and the corresponding trivalent metal were initially disordered over the four belt positions of the polyoxometalate clusters (two internal and two external), and their population parameters were refined without restrictions. In the case of **2-Sc**, a Sc/W population of 50/50 was obtained for the external sites. This crystallographic disorder has been previously observed in related compounds.[30] In **2-Mn**, 100% Mn and 100% W populations were obtained for the external and the internal sites, respectively.

2.2.4. Powder X-ray diffraction (PXRD)

Powder X-ray diffraction (PXRD) patterns were collected from 2θ = 4 to 60° (0.02606° step size, 30s per step) using a Philips X'PERT PRO diffractometer operating with monochromated Cu Kα radiation (λ = 1.5418 Å).

2.2.5. Elemental analysis (CHN)

Carbon and hydrogen contents for **1-Fe** were determined on a EuroVector EA 3000 CHNSO analyser from the Central Analysis Service of Bizkaia (SCAB) belonging to SGIker, University of the Basque Country UPV/EHU.

2.2.6. Electron paramagnetic resonance spectroscopy (EPR)

The electron paramagnetic resonance (EPR) spectra for **1-Fe** and **2-Mn** were recorded on powdered crystalline samples at X-band frequency by using a Bruker ELEXSYS 500 spectrometer equipped with a superhigh-Q resonator ER-4123-SHQ and a standard

Oxford-low temperature device. The magnetic field in the equipment was calibrated with an NMR probe. The frequency inside the cavity was measured with a Hewlett-Packard 5352B microwave frequency counter.

3. RESULTS AND DISCUSSION

3.1. GENERAL SYNTHETIC CONSIDERATIONS

This section summarizes all the results obtained in the systematic studies on the reactivity of the lacunary $[SbW_9O_{33}]^{9-}$ POM towards different trivalent metals. The isolated novel compounds have been chemical and structurally characterised as described in the following sections.

The reactivity of the Keggin-type B-α-SbW$_9$ trilacunary polyoxoanion towards trivalent metals (M^{III} = Cr, Mn, Fe, Co, Al, Ga) has been evaluated following the reported synthetic procedure for the preparation of divalent-metal disubstituted Krebs-type POMs.[29] FT-IR spectroscopic analyses were carried out on any solid sample (crystalline or not) obtained by slow evaporation of the final solutions at room temperature, as it is a very straightforward and powerful tool for the identification of the resulting polyoxoanions.

First, the studies were focused on the reaction with FeCl$_3$·6H$_2$O. The synthetic method involving a POM:Fe ratio of 1:1.5 in a 1 mol L^{-1} acetic acid/sodium acetate buffer (pH = 4.7) at 40 °C led to the novel compound **1-Fe**. This compound contains the iron-trisubstituted $[\{Fe(C_2H_3O_2)\}_3(SbW_9O_{33})_2]^{12-}$ Hervé-type POM according to FT-IR spectroscopy (see section 3.2). It constitutes the first evidence of Fe substitution into a Hervé-type anion, and represents the second example of the incorporation of a trivalent metal ion into the Hervé-type skeleton, after the previously reported Mn^{III} derivative.[26] Following a similar synthetic procedure but using divalent metals, Piepenbrink et al.[29] obtained the disubstituted $[\{Mn(H_2O)_3\}_2(WO_2)_2(SbW_9O_{33})_2]^{10-}$ Krebs-type POM for Mn^{II} and Zn^{II}. This fact suggests that the reactivity of trivalent metals towards the B-α-SbW$_9$ trilacunary POM is very different from that of the divalent ions.

Additional experiments were conducted in aqueous media to check the influence of the pH. The range was limited to pH = 2-6 and the tetrasubstituted Krebs-type POM $[Fe_4^{III}(H_2O)_{10}(SbW_9O_{33})_2]^{6-}$ was obtained in all cases as identified by FT-IR spectroscopy (Figure 8). At low pH values (2 to 4) yellow plates were obtained, whereas higher pH values in the 5-6 range yielded the compound as a powdered solid with low crystallinity which could not be properly identified on the basis of FT-IR spectroscopy. The FT-IR spectra of the yellow plate-like crystals are virtually identical (Figure 9) and display bands that match those observed for the iron-tetrasubstituted Krebs-type POM obtained by Kortz et al. [IR (KBr): $\bar{\nu}$ (cm^{-1}): 949 (m), 881 (m), 805 (s), 771 (s), 669 (w)].[42] These results are in good agreement with previous studies by Kortz, who obtained this POM using a different stoichiometric ratio at pH = 3.0,[42] and by Krebs, who reported the $\alpha \rightarrow \beta$ isomerization of the $(XW_9O_{33})^{n-}$ trilacunary polyanions at low pH.[14]
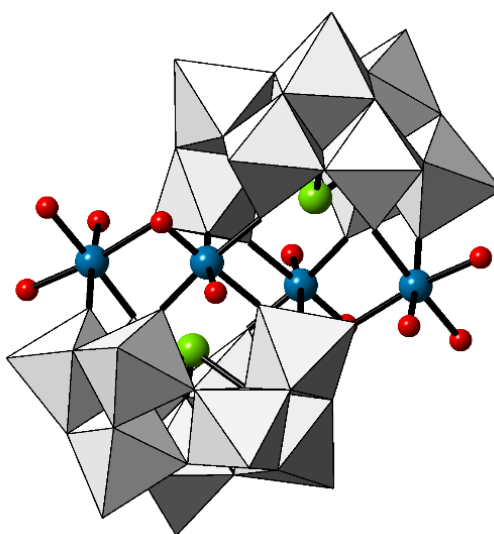

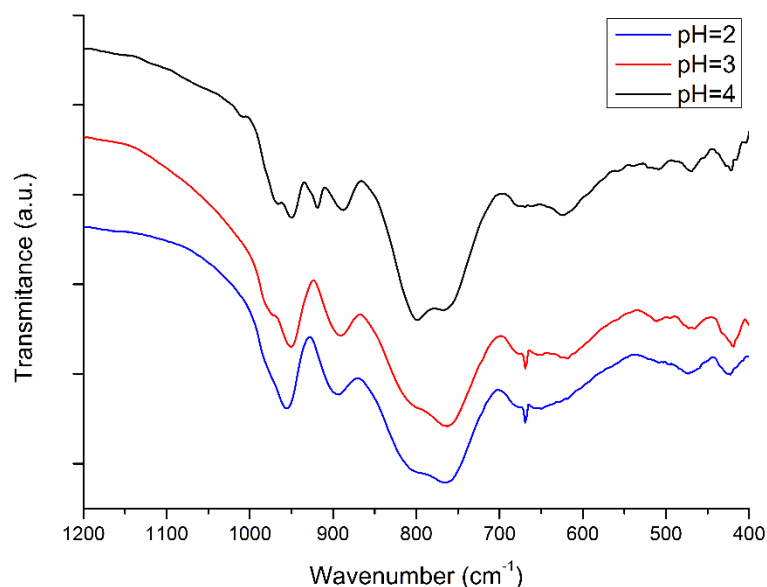*Figure 8.- Molecular structure of the tetra-iron(III)-substituted Krebs-type POM.*

Figure 9.- FT-IR spectra of the tetra-iron(III)-substituted Krebs-type POM obtained in the pH = 2-4 range.

The results obtained using the original synthetic conditions (1 mol L^{-1} NaAc/HAc buffered medium, pH = 4.7) encouraged us to perform additional experiments by substituting Fe^{III} with some other 3d- (Sc^{III}, Cr^{III}, Mn^{III}, Co^{III}) or p-block (Al^{III}, Ga^{III}) metals. The reaction turned out to be really dependent on the specific nature of the trivalent metal because: (i) for Co, Al or Ga there is no metal incorporation and the corresponding non-substituted polyoxotungstate is obtained as a sodium salt; or (ii) the reaction with trivalent metals takes place and the corresponding metal-substituted sandwich-type POM is obtained. Most of these experiments yielded single crystals suitable for X-ray diffraction. The cases in which crystallographic evidences (full data acquisition or unit cell determination) were acquired are summarized in Scheme 1.

Scheme 1.- Summary of the results obtained for the reactions between the Keggin-type SbW$_9$ trilacunary polyoxoanion and different trivalent metals (M^{III} = Fe, Sc, Mn, Al, Ga) in which crystallographic information was obtained. Colour code: same as in previous Figures, but for C, black and H, white.
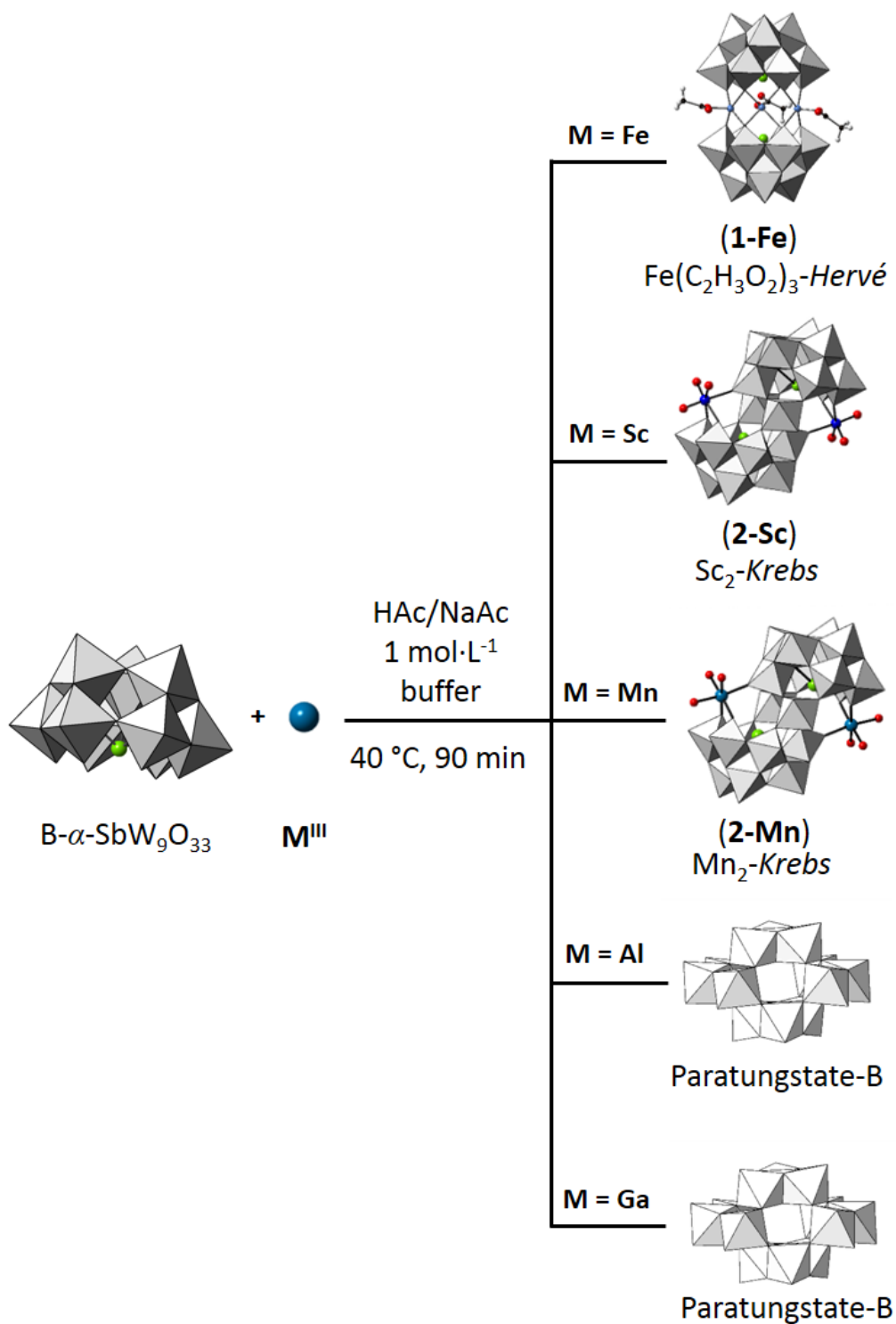
The use of Sc[III] and Mn[III] salts led to the formation of a Krebs-type POM according to FT-IR spectroscopy (see section 3.2). As shown by the XRD experiments (see section 3.4), **2-Sc** and **2-Mn** represent unprecedented compounds, that is, their structures do not correspond to any of the cell parameters included in the ICSD crystallographic database.[43] Thus, their full characterisation will be described in the following sections. Moreover, compound **2-Sc** is the second example of a scandium-substituted POM, the first one being a silicotungstate hybrid species reported by Zhang et al.[44] The crystallographic studies also show that the amount of scandium incorporated into the POM structure in **2-Sc** is less than expected, which could be related with the low solubility in the buffered medium of the Sc_2O_3 reagent used for availability reasons. Therefore, the synthesis will be repeated in the near future using a more soluble Sc[III] salt (nitrate, chloride) in order to solve this problem. For **2-Mn**, the 3d metal underwent a reduction process during the synthesis according to single-crystal X-ray diffraction experiments (see section 3.4). The presence of Mn[II] was further confirmed by EPR spectroscopy (see section 3.6).
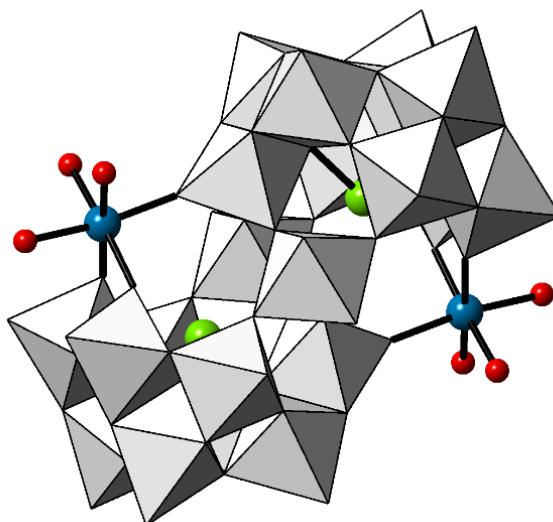

*Figure 10.- Molecular structure of **2-M** (M = Sc, Mn)*

The use of p-block trivalent metal (Al^{III} and Ga^{III}) nitrates led to the isolation of paratungstate-B $[W_{12}O_{40}(OH)_2]^{10-}$ iso-POM. The reaction for both Al^{III} and Ga^{III} initially resulted in colourless crystals that were preliminarily characterised by FT-IR spectroscopy. The obtained spectra were similar to that of the paratungstate-B sodium salt reported by Chrissafidou et al.[45], which was prepared *ex profeso* for comparative purposes (Figure 11). For both compounds, the $W-O_t$ and $W-O_b$ stretching vibrational bands appear at ca. 940 cm^{-1}, and in the 600-900 cm^{-1} range, respectively. The latter include at least four signals of strong intensity at ca. 874, 845, 800 and 712 cm^{-1}. Although all the FT-IR spectra show the characteristic bands of the paratungstate-B ion, the slight differences between them could originate from different crystal packings, or from the presence of Al or Ga atoms acting as counterions in the structure.
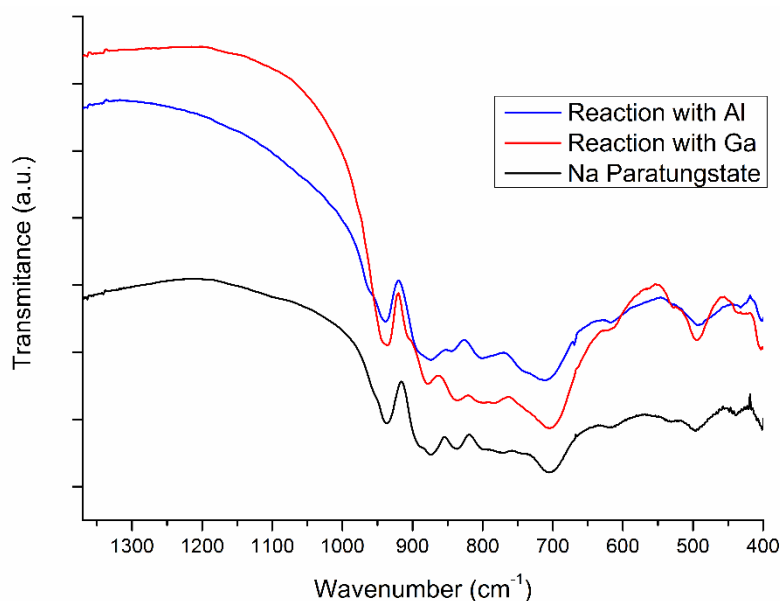

Figure 11.- FT-IR spectra of the paratungstate-B iso-POM compared with those of the crystals obtained from the reactions with Al and Ga.

After the spectroscopic characterisation, XRD experiments were conducted on a single-crystal obtained from the reaction carried out with the aluminium salt to determine whether the aluminium cations were present in the structure. Preliminary

experiments for the unit cell determination revealed virtually identical unit cell parameters compared with those reported for Chrissafidou's compound $Na_{10}[W_{12}O_{40}(OH)_2] \cdot 27H_2O$. A full data acquisition was performed and the resolution of the crystal structure led to the following crystal data: $H_{96}Na_{10}O_{89}W_{12}$, FW = 3540.10 g mol^{-1}, triclinic, *P-1* space group, *a* = 11.7699(4) Å, *b* = 12.4083(5) Å, *c* = 22.0351(9) Å, α = 86.306(3)°, β = 86.602(3)°, γ = 66.482(4)°, *V* = 2942.7(2) $Å^3$, *T* = 100(2) K, *Z* = 2, D_{calcd} = 3.995 g cm^{-3}, μ = 23.557 mm^{-1}, 22006 reflections collected, 11823 unique (R_{int} = 0.043), 10561 observed [$I > 2\sigma(I)$], 425 parameters, *R(F)* = 0.058 [$I > 2\sigma(I)$], $wR(F^2)$ = 0.148 (all data), GoF = 1.113. The single crystals obtained from the reaction with Ga^{III} were found to show the same unit cell parameters according to XRD experiments.

The molecular structure of the paratungstate-B iso-POM is shown in Figure 12. This cluster is centrosymmetric, and it is formed by twelve {WO_6} units that are arranged in four distinct trimeric subunits assembled by corner sharing. There are two types of subunits: top and bottom {W_3O_{13}} groups are formed by edge-sharing octahedra, whereas the central {W_3O_{14}} groups show a {WO_6} octahedral unit linked to two adjacent analogous units *via* edge-sharing. The structure is stabilized by the protonation of the two central O atoms.[9]
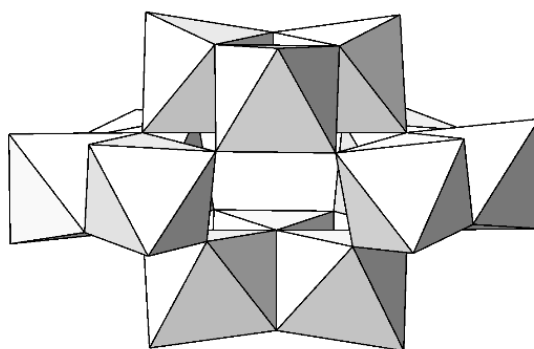

Figure 12.- Molecular structure of paratungstate-B iso-POM.

Regarding the reactions for which no crystalline samples were obtained, that using $Cr(NO_3)_3 \cdot 9H_2O$ led to a powdered green solid, which according to FT-IR, is based on the $[Cr_4(H_2O)_{10}(SbW_9O_{33})_2]^{6-}$ tetrasubstituted Krebs-type POM reported by Kortz.[42] This compound has the same molecular structure as the tetra-iron(III)-substituted Krebs-type cluster shown in Figure 8. The identification was carried out by the comparison of the FT-IR spectrum of the green powder with that recorded for the crystalline product of the previously mentioned reaction carried out with the iron salt in aqueous acidic conditions (pH = 2) (Figure 13).
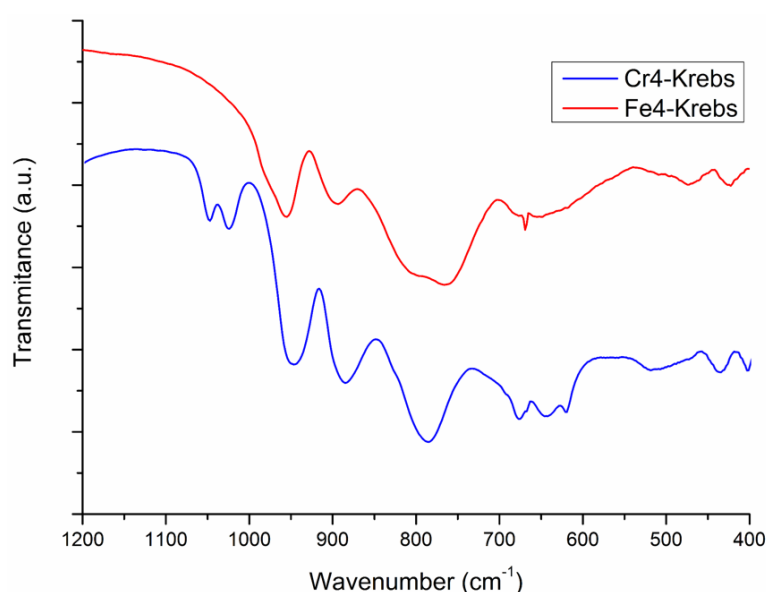

Figure 13.- FT-IR spectrum of the tetra-chromium(III)-substituted Krebs-type POM compared to the tetra-iron(III)-substituted analogue.

In regard to the reaction with the Co^{III} precursor, the use of *Co(acac)₃* afforded a mixture of green needles and colourless crystals that were identified by means of FT-IR. The spectrum of the green crystals exhibits the presence of bands in the organic region (> 1200 cm^{-1}) together with the absence of any POM structure in the inorganic region (< 1200 cm^{-1}). Its comparison with the spectrum of the commercial $Co(acac)_3$ revealed that these green crystals corresponded to the acetyl acetonate precursor that did not react with the trilacunary Keggin-type POM (Figure 14a). Moreover, the IR spectrum of the colourless crystals resembles the shape of the well-known Krebs-

type structure. However, these colourless crystals contain impurities of the cobalt complex, as they show several vibrational bands in the organic region (Figure 14b). The colourless nature of the product, together with the similarity of its spectrum with that of the tungsten-containing $[\{WO_2(OH)_2\}(WO_2)_2(B\text{-}\beta\text{-}SbW_9O_{33})_2]^{12-}$ species (W_4-Krebs) prepared for comparative purposes following reported procedures,[14] suggests that this product is based on the $[\{WO_2(OH)_2\}(WO_2)_2(B\text{-}\beta\text{-}SbW_9O_{33})_2]^{12-}$ Krebs-type anion.
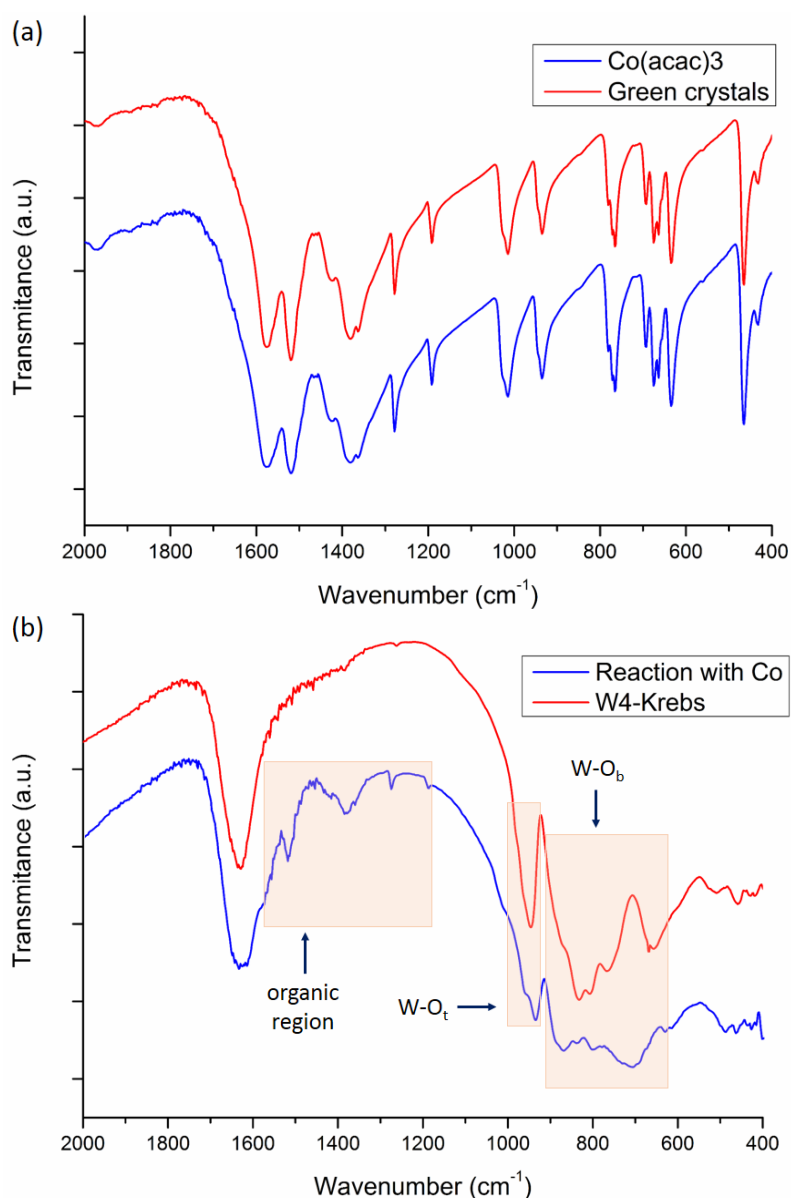

Figure 14.- (a) FT-IR spectrum of the green needle-like crystals compared with that of the Co(acac)₃ precursor; (b) FT-IR spectrum of the colourless crystals compared with the W₄-Krebs POM containing exclusively tungsten.

The spectroscopic (FT-IR), thermal (TG), and structural characterisation of the novel compounds **1-Fe**, **2-Sc** and **2-Mn** is detailed in the following sections. The last part deals with a more sophisticated characterisation technique like the EPR spectroscopy, which has been used to confirm different assumptions taken with regard to the oxidation states of the Fe and Mn centres in compounds **1-Fe** and **2-Mn**.

3.2. SPECTROSCOPIC CHARACTERISATION

Compounds **1-Fe**, **2-Sc** and **2-Mn** were analysed by FT-IR spectroscopy prior to X-ray diffraction studies. The FT-IR spectra for the sandwich-type compounds **1-Fe** and **2-M** (M = Sc, Mn) are shown in Figures 15 and 16, respectively.

Two regions can be clearly differentiated in the FT-IR spectrum of **1-Fe**. The organic region above 1200 cm^{-1} shows two bands at 1377 and 1317 cm^{-1} that correspond to COO stretching and CH_3 bending vibrations of acetate ligands coordinated in a monodentate fashion.[46] The POM region below 1200 cm^{-1} displays the v_{as} (W-O_t) and v_{as} (W-O_b-W) bands characteristic of a 3d-metal trisubstituted Hervé-type POM at 949, 868, 737 and 689 cm^{-1}. The comparison of the spectrum with that of $[Cu(H_2O)_3(SbW_9O_{33})_2]^{n-}$, prepared exclusively for comparative purposes following a reported procedure,[19] shows a change in the relative intensity of the bands, as well as small red shift for the W-O_b-W stretching bands of about 5 cm^{-1}. There is a shoulder at 780 cm^{-1} in the spectra of Cu_3-Hervé that disappears for **1-Fe**, and a new one appears at 680 cm^{-1}.

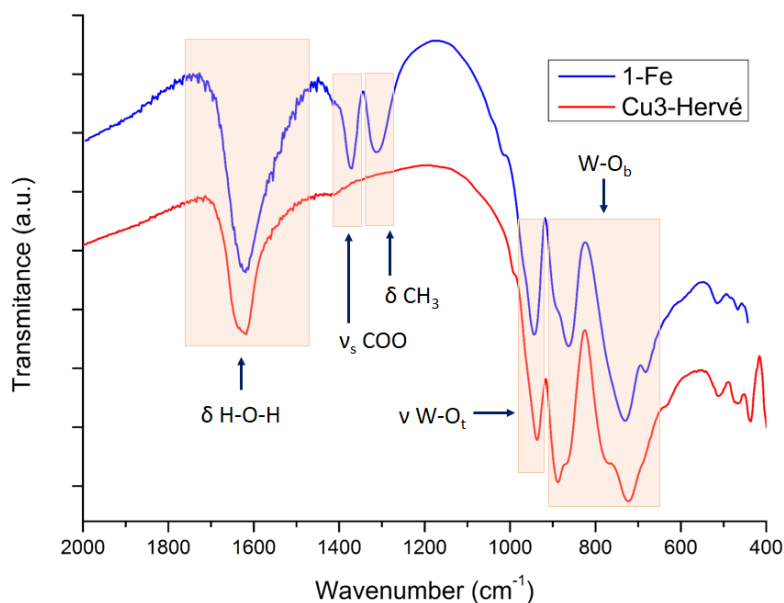*Figure 15.- FT-IR spectrum of **1-Fe** and its comparison with that of Na$_9$[Cu(H$_2$O)$_3$(SbW$_9$O$_{33}$)$_2$]·nH$_2$O (O$_t$, terminal oxygen; O$_b$, bridging oxygen; ν, stretching; δ, bending).*

Similar spectra were obtained for **2-Sc** and **2-Mn**, which display characteristic bands of the well-known Krebs-type skeleton with signals at 957, 841, 804 and 758 cm^{-1} that correspond to ν$_{as}$ (W-O$_t$) and ν$_{as}$ (W-O$_b$-W) antisymmetric stretching vibrations. Because of their formal double bond character, W-O$_t$ bands are observed at higher wavenumbers in the 1000-900 cm^{-1} range, whereas W-O$_b$ stretching bands involving bridging O atoms appear in the 850-650 cm^{-1} range.[29,47]

The spectrum of **2-Mn** is virtually identical to that of the [{Mn(H$_2$O)$_3$}(WO$_2$)$_2$(SbW$_9$O$_{33}$)$_2$]$^{10-}$ (*Mn$_2$-Krebs*) anion.[29] However, a small difference is observed in both the position and the relative intensity of the bands in comparison to those observed for **2-Sc**. This change might be due to the presence of a mixture of exclusively tungsten containing and the Sc^{III} disubstituted Krebs-type POM in the crystal structure of **2-Sc**, as observed in single-crystal X-ray diffraction experiments.
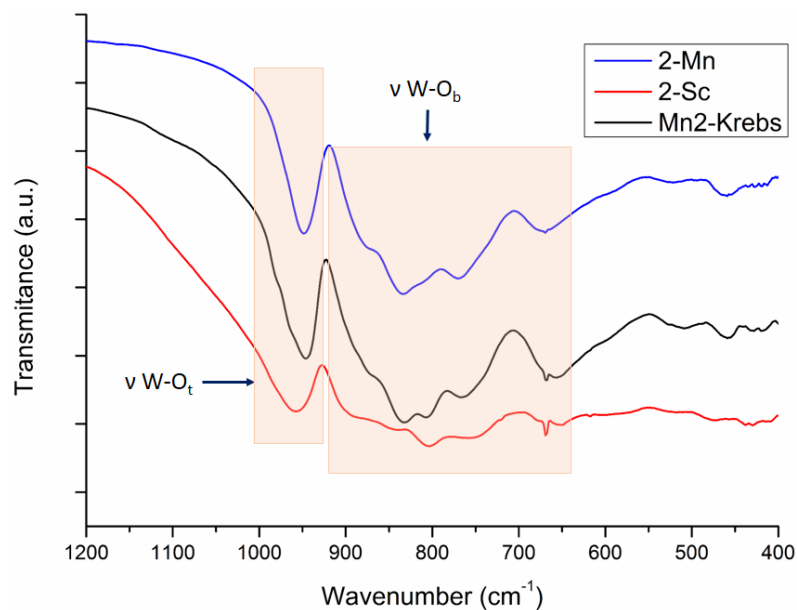
*Figure 16.- FT-IR spectra of **2-Sc** and **2-Mn** compared to that of compound*
Na$_{10}$[{Mn(H$_2$O)$_3$}(WO$_2$)$_2$(SbW$_9$O$_{33}$)$_2$]·nH$_2$O (Mn$_2$-Krebs).

3.3. THERMAL ANALYSIS

Thermogravimetry (TG) is based on the measurement of the mass variation of a sample kept in a controlled furnace whose temperature is gradually raised under a controlled atmosphere. A plot of mass as a function of temperature represents the essential thermogravimetric result.[48] TG curves registered for **1-Fe**, **2-Sc** and **2-Mn** are shown in Figure 17.

Thermal decomposition of **1-Fe** occurs in two different stages. The first step corresponds to an endothermic dehydration process which proceeds *via* continuous mass loss and it is completed at ca. 330 °C. This process involves the release of ca. 36 water molecules [% mass, calcd (found) for 36 H$_2$O molecules: 11.0 (11.0)]. The final step corresponds to the organic ligand combustion and decomposition of the POM fragment, and is completed at ca. 400 °C. This step involves the release of three acetate units [% mass, calcd (found) for 3 C$_2$H$_3$O$_2$ groups: 3.0 (2.7)]. The resulting final residue compares well with that calculated for a mixture of oxides [%mass, calcd (found) for Fe$_3$Na$_{12}$O$_{68}$Sb$_2$W$_{18}$: 86.5 (86.3)].

Thermogravimetric analyses show TG curves with similar profiles for both **2-Sc** and **2-Mn**. The first weight loss corresponds to an endothermic dehydration process, which proceeds *via* continuous mass loss and it is completed at around 200-210 °C for both compounds, comprising the loss of ca. 14% and 12% of the total mass, which accounts for 50 and 41 water molecules, respectively [%mass, calcd (found) for 50 and 41 H_2O molecules, respectively: 14.0 (14.0) for **2-Sc** and 12.1 (12.0) for **2-Mn**]. The final step corresponds to the POM breakdown, which is completed at temperatures in the 600-640 °C range, resulting in the final residue [%mass, calcd (found) for the final residue: $Na_{10}O_{73}Sb_2ScW_{21}$: 86.0 (85.2) for **2-Sc**; $Na_{10}O_{70}Sb_2Mn_2W_{20}$: 87.9 (86.8) for **2-Mn**].
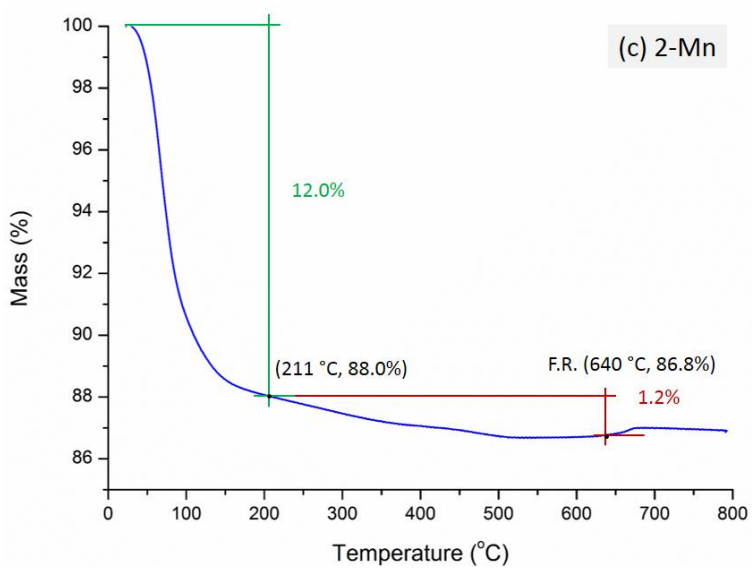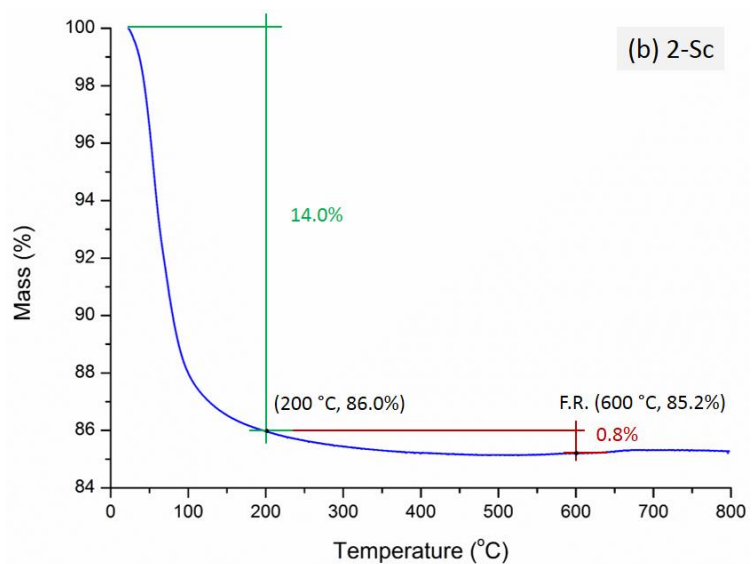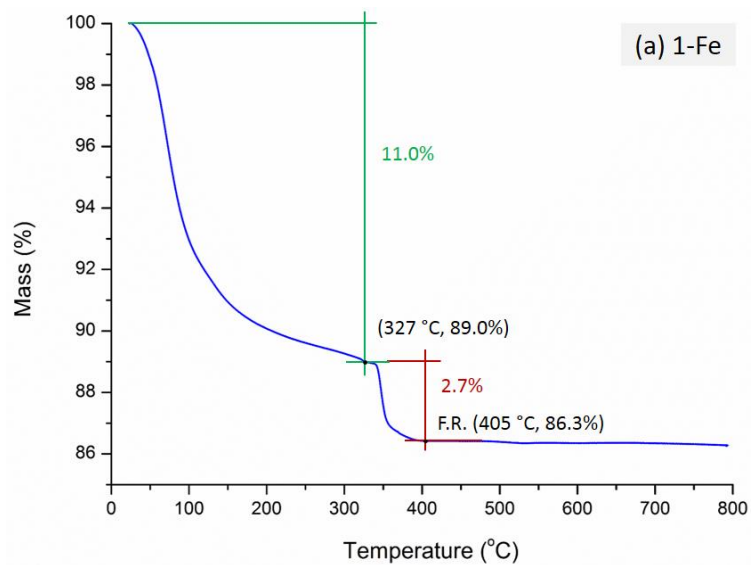
*Figure 17.- TG curves for (a) **1-Fe**, (b) **2-Sc** and (c) **2-Mn**. F.R. stands for final residue.*

3.4. CRYSTAL STRUCTURE

Crystallographic data for compounds **1-Fe** and **2-M** (M = Sc, Mn) are summarized in Table 1.

*Table 1.- Crystallographic data for compounds **1-Fe** and **2-M** (M = Sc, Mn).*

	1-Fe	2-Sc	2-Mn
Formula	$C_6H_{81}Fe_3Na_{12}O_{108}$ Sb_2W_{18}	$H_{101}Na_{10}O_{123}Sb_2$ ScW_{21}	$H_{82}Mn_2Na_{10}O_{111}$ Sb_2W_{20}
FW (g mol^{-1})	5877.7	6448.7	6118.7
Crystal system	triclinic	monoclinic	monoclinic
Space group	*P–1*	*C2/c*	*P2$_1$/n*
***a* (Å)**	17.7478(4)	34.1426(16)	18.9916(3)
***b* (Å)**	22.3796(5)	25.7316(6)	16.39535(19)
***c* (Å)**	26.1824(10)	13.0248(6)	19.1797(4)
***α* (°)**	92.376(2)	90.00	90.00
***β* (°)**	98.687(3)	92.316(5)	116.959(2)
***γ* (°)**	97.261(2)	90.00	90.00
***V* (Å^3)**	10178.2(5)	11433.5(8)	5323.08(15)
Z	4	4	2
***D*$_{calcd}$ (g cm^{-3})**	3.836	3.746	3.818
***μ* (mm^{-1})**	21.361	43.544	22.397
Reflections			
Collected	68551	2275	36198
Unique (*R*$_{int}$)	35825 (0.110)	1299 (0.047)	10730 (0.037)
Observed [*I* > 2σ(*I*)]	21849	1159	8347
Parameters	1421	366	321
***R(F)*[a] [*I* > 2σ(*I*)]**	0.101	0.043	0.070
***wR(F^2)*[a] (all data)**	0.309	0.120	0.226
GoF	0.987	1.106	1.031

[a] $R(F) = \Sigma||F_o - F_c||/\Sigma|F_o|$; $\omega R(F^2) = \{\Sigma[\omega(F_o{}^2 - F_c{}^2)^2]/\Sigma[\omega(F_o{}^2)^2]\}^{1/2}$

Compound **1-Fe** crystallizes in the triclinic space group *P-1*, and the asymmetric unit contains two $[\{Fe(C_2H_3O_2)\}_3(SbW_9O_{33})_2]^{12-}$ sandwich-type POM units together with twelve sodium cations and 36 water molecules of hydration per cluster. The molecular structure of each sandwich-type POM shows the well-known Hervé-type structure and it is formed by two B-α-SbW$_9$ trilacunary units enclosing three iron(III) centres in a square-based pyramid geometry. The coordination environment of each metal centre is completed by two oxygen atoms from each B-α-SbW$_9$O$_{33}$ unit, and an apical oxygen from an acetate ligand coordinated in a monodentate fashion. The metallic centres in compound **1-Fe** are trivalent, in good agreement with the number of Na cations located in the structure. This was further confirmed by EPR spectroscopy (see section 3.6). Each metallic centre in the structure is coordinated to an acetate group, leading to an {Fe^{III}-acetate} moiety, which has a formal charge of 2+. The fact that most examples of substituted Hervé-type POMs found in the literature are for divalent metals may account for the high yield obtained in the synthesis of compound **1-Fe**.
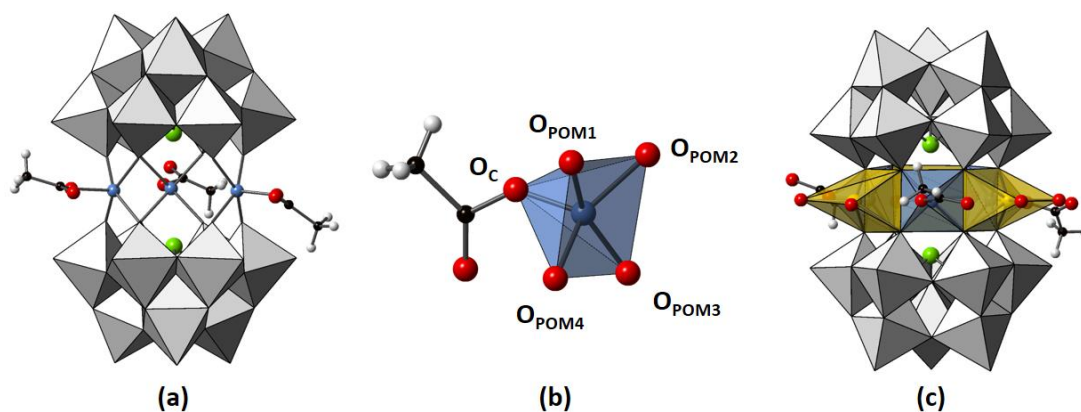

*Figure 18.- (a) Molecular structure of sandwich-type POMs in **1-Fe** together with (b) the coordination geometry for the metal centres (labels: O$_c$, acetate oxygen atom; O$_{POM}$, oxygen atoms belonging to the B-α-SbW$_9$ units). (c) The coordination polyhedra of belt Na cations are highlighted in yellow.*

Although the ideal metal substituted Hervé-type structure shows a three-fold rotation axis (C_{3v}), in the case of **1-Fe**, the symmetry is broken by the different crystallographic arrangements adopted by the acetate groups. The remaining three belt positions are occupied by sodium cations containing two additional coordinated water molecules of hydration. The coordination geometry of the Fe^{III} centres is shown in Figure 18, along with the molecular structure of **1-Fe**. The Fe–O bond lengths are summarized in Table 2.

*Table 2.- Bond lengths (Å) of the coordination spheres of the Fe^{III} centres in **1-Fe**.*

POM unit	Fe	Fe–O_C	Fe–O_{POM1}	Fe–O_{POM2}	Fe–O_{POM3}	Fe–O_{POM4}
1	Fe1	1.87(3)	1.91(2)	1.93(2)	1.994(19)	1.92(2)
	Fe2	1.91(2)	1.95(3)	1.97(2)	1.96(2)	1.98(2)
	Fe3	1.92(3)	1.924(18)	1.91(2)	1.967(17)	1.98(2)
2	Fe4	1.85(3)	2.03(3)	1.988(19)	2.01(3)	1.96(2)
	Fe5	1.90(2)	1.95(2)	1.97(2)	1.93(2)	1.94(2)
	Fe6	1.86(3)	1.98(2)	2.02(2)	1.91(2)	1.97(2)

One dimensional ribbon-like arrangements of Hervé-type POMs running along the *x* axis can be found in the crystal packing of **1-Fe**. These ribbons are formed by two zig-zag rows of crystallographically independent clusters arranged in an antiparallel fashion, which are connected to each other *via* weak C–H···O_{POM} type hydrogen bonds involving methyl groups of the acetate ligand and O_{POM} atoms (Figure 19). Geometrical parameters of the intermolecular C–H···O interactions are summarized in Table 3.

*Table 3.- Geometrical parameters (Å, °) for the intermolecular C–H⋯O hydrogen bonds involving the methylic C atoms of the acetate group and the O_{POM} atoms in compound **1-Fe** (D, donor; H, hydrogen; A, acceptor).*

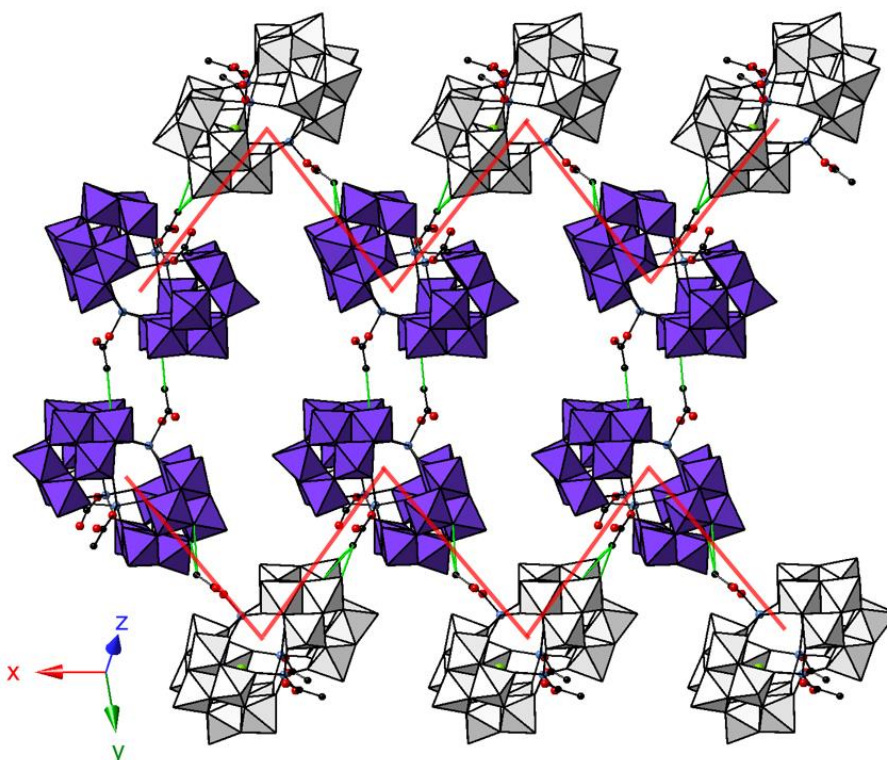| D–H⋯A	H⋯A	D⋯A	<D–H⋯A>
C–H⋯O	H⋯O_{POM}	C⋯O_{POM}	C-H⋯O_{POM}
C6–H6B⋯O105[i]	2.85	3.17(4)	144
C10–H10C⋯O89[ii]	2.86	3.50(6)	123
C10–H10C⋯O58[ii]	2.61	3.45(5)	144
C4–H4A⋯O35T	2.41	3.03(4)	121
C4–H4B⋯O32T	2.37	3.12(4)	134
C4–H4B⋯O325	2.49	3.16(4)	125

Symmetry codes: (i) –x, 1 – y, 1 – z; (ii) 1 + x, y, z.

*Figure 19.- View of the crystal packing of **1-Fe** along the [011] direction. {WO₆} octahedra from the two crystallographically independent clusters are depicted in grey and blue, respectively. The C–H⋯O_POM bonds are shown in green colour. The red lines illustrate the one-dimensional assembly of the two zig-zag rows arranged in antiparallel fashion.*

Compounds **2-Sc** and **2-Mn** crystallize in the monoclinic *C*2/*c* and *P*2₁/*n* groups, respectively. Both consist on hydrated sodium salts of the well-known [{M(H$_2$O)$_3$}$_2$(WO$_2$)$_2$(SbW$_9$O$_{33}$)$_2$]$^{n-}$ metal-disubstituted Krebs-type POM clusters. These are composed of two trilacunary Keggin [B-β-SbW$_9$O$_{33}$]$^{9-}$ subunits linked *via* corner sharing by two internal {WO$_6$} octahedra (each showing two *cis*-related terminal O atoms) and two M atoms coordinated at external positions to two O$_{POM}$ atoms that belong to a {W$_2$O$_{11}$} corner-shared fragment of one subunit and to an additional O$_{POM}$ atom from the 60°-rotated {W$_3$O$_{13}$} trimer of the second subunit. The coordination spheres of the octahedral M metal centres are completed with three water molecules in a relative *fac*-arrangement (Figure 20). The M–O bond lengths for the coordination spheres of the external Sc and Mn centres for **2-Sc** and **2-Mn**, respectively, are included in Table 4.

*Table 4.- Summary of bond lengths (Å) found for the metal centres in compounds **2-Sc** and **2-Mn**.*

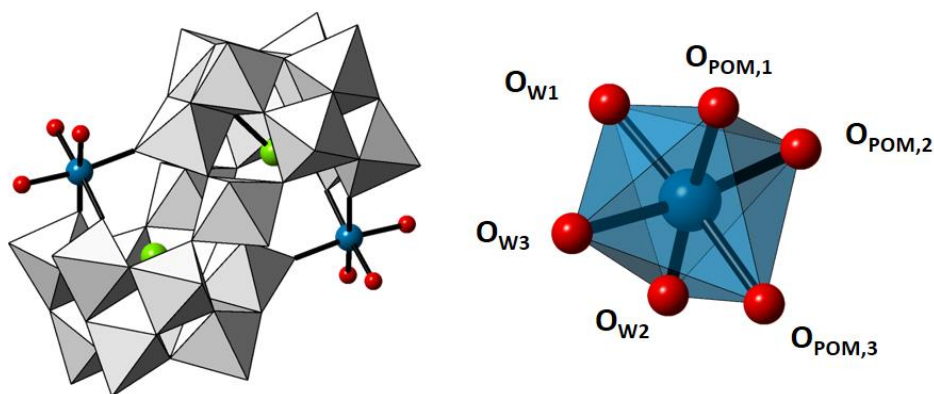|	M-O$_{W1}$	M-O$_{W2}$	M-O$_{W3}$	M-O$_{POM1}$	M-O$_{POM2}$	M-O$_{POM3}$
Sc	1.88(4)	2.04(4)	1.82(5)	2.04(4)	2.22(4)	2.26(5)
Mn	2.208(15)	2.194(14)	2.170(19)	2.141(13)	2.103(12)	2.120(14)

*Figure 20.- Left: Molecular structure of disubstituted sandwich-type POMs in **2-M** (M = Sc, Mn). Right: The coordination geometry of the outer belt metal centres (labels: O$_W$, water molecules; O$_{POM}$, oxygen atoms belonging to the B-α-SbW$_9$ subunit).*

The polyanions in **2-Sc** display a severe Sc/W crystallographic disorder in their respective external belt positions corresponding to a 50% population per each centre. The {Sc(H$_2$O)$_3$}$^{3+}$/{WO$_2$(OH)}$^+$ partial substitution is in good agreement with the total number of ten sodium cations located in the crystal structure. For comparison, Piepenbrink et al.[29] reported external W occupancies of 20% for the [{Zn^{II}(H$_2$O)$_3$}$_2$(WO$_2$)$_2$(SbW$_9$O$_{33}$)$_2$]$^{10-}$ derivative demonstrating that such kind of substitution is usual in this family of POMs. To date, there is no evidence of a monosubstituted Krebs-type POM in the literature. These facts suggest that the crystal structure of **2-Sc** is composed by a 50% mixture of the scandium disubstituted Krebs-type anions [{Sc^{III}(H$_2$O)$_3$}$_2$(WO$_2$)$_2$(SbW$_9$O$_{33}$)$_2$]$^{8-}$ and the exclusively tungsten containing analogue [{WO$_2$(OH)}$_2$(WO$_2$)$_2$(SbW$_9$O$_{33}$)$_2$]$^{12-}$ resulting in the general formula [{Sc^{III}(H$_2$O)$_3$}{WO$_2$(OH)}(WO$_2$)$_2$(SbW$_9$O$_{33}$)$_2$]$^{10-}$ reported in this work. The structural disorder could originate from the low solubility of the Sc$_2$O$_3$ used in the reaction. Therefore, the use of a more soluble Sc^{III} precursor in the synthetic procedure could solve this problem.

In regard to the polyanions in **2-Mn**, they are virtually identical to those reported by Piepenbrink et al. for the Mn^{II} disubstituted [{Mn^{II}(H$_2$O)$_3$}$_2$(WO$_2$)$_2$(SbW$_9$O$_{33}$)$_2$]$^{10-}$ derivative which showed no crystallographic W/Mn disorder in the outer belt positions.[29] The reduction of the Mn centres from the +3 oxidation state in the Mn(C$_5$H$_7$O$_2$)$_3$ precursor to +2 in **2-Mn** is in good agreement with the 5 sodium cations per one half of the sandwich-type POM found in XRD experiments. This observation was further confirmed by EPR experiments (see Section 3.6). Consequently, **2-Mn** (Monoclinic, $P2_1/n$: a = 18.9916(3), b = 16.39535(19), c = 19.1797(4), β= 116.959(2). V = 5323.08(15) Å^3) can be regarded as a new polymorph of the Piepenbrink's anion with a different degree of hydration (34 H$_2$O molecules for compound **2-Mn**; 40 H$_2$O molecules for the reported compound).

The crystal packing of both structures show the hybrid POMs packed following different structural motifs: compound **2-Sc** exhibits a diamond-like motif, whereas **2-Mn** displays a brick-wall pattern (Figure 21).
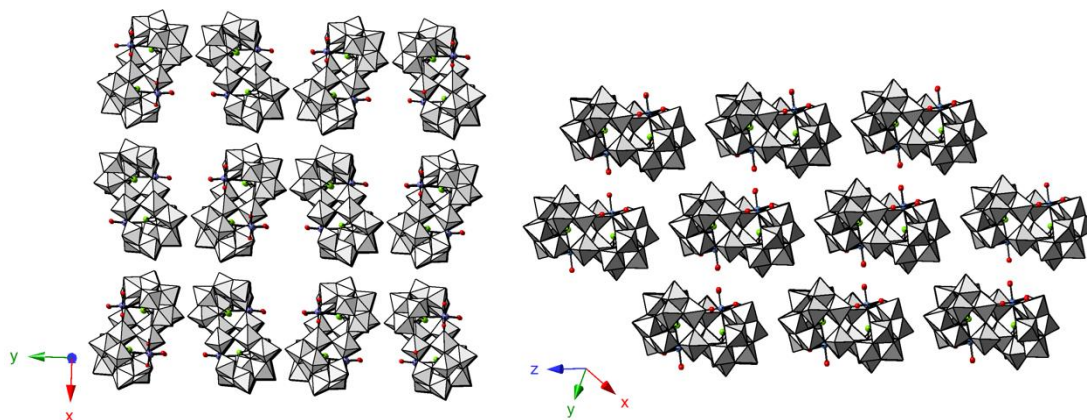
*Figure 21.- View of the crystal packing of the polyanions along the [010] direction for **2-Sc** (left) and the [1-11] direction for **2-Mn** (right).*

3.5. X-RAY DIFFRACTION ON POWDERED SAMPLES

The powder X-ray diffraction pattern for **1-Fe** was recorded and compared to the simulated diffractogram obtained from the single-crystal XRD measurement, which was generated using Mercury® 3.5.1 software (Figure 22). Considering the great similarity between diffraction patterns, it can be concluded that the major crystalline phase (>95%) in the sample is that of **1-Fe**.
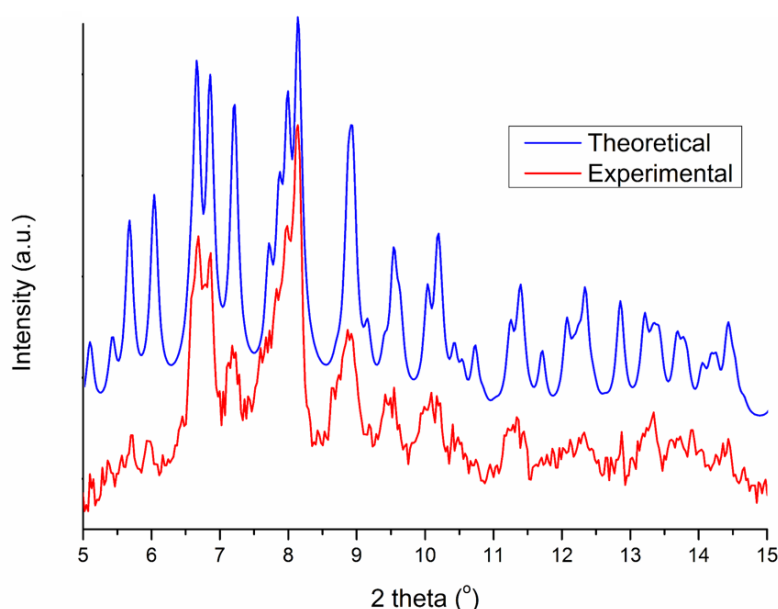

*Figure 22.- Powder X-ray diffraction pattern for **1-Fe** compared to that simulated from the single-crystal X-ray diffraction data.*

3.6. ELECTRON PARAMAGNETIC RESONANCE SPECTROSCOPY

Electron Paramagnetic Resonance (EPR) (or Electron Spin Resonance, ESR) spectroscopy is a technique employed for the study of systems that contain unpaired electrons including paramagnetic centres and radical species. Each paramagnetic metal centre produces a characteristic EPR signature.[49] However, the EPR signal is highly dependent on the coordination environment of the metal ions and the magnetic coupling with other centres.

EPR spectra were recorded at X-band frequency, at 5K for **1-Fe** and at room temperature for **2-Mn** (Figure 23). In both cases the spectra were complicated to analyse due to (i) the presence of more than one metallic centre, and (ii) the distorted octahedral coordination geometry of the metal centres within the POM skeleton. The results obtained were useful to confirm the presence of both Fe^{III} and Mn^{II} in the molecular structures of **1-Fe** and **2-Mn**, as the Fe^{II} ($3d^6$) and Mn^{III} ($3d^4$) species would not show any EPR signal.[50]
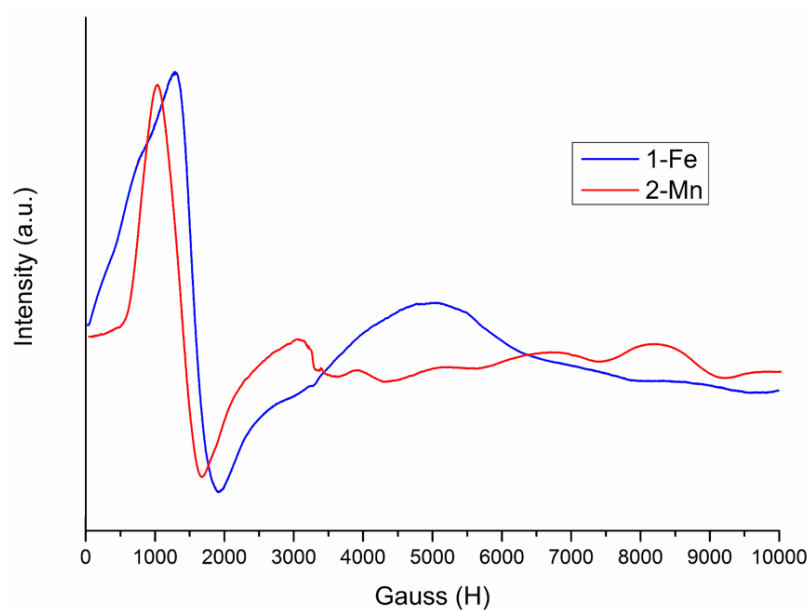

*Figure 23.- EPR spectra of compounds **1-Fe** and **2-Mn**.*

4. CONCLUSIONS

This work affords further insight into the reactivity of the Keggin-type $[B-\alpha-SbW_9O_{33}]^{9-}$ trilacunary anions with diverse trivalent metals because their behaviour has been found to be very different to that shown by the more studied divalent metals. The reactivity of the metal centres in a sodium acetate buffered media has proven to be extremely dependent on their nature, in such a way that, (i) there is no reaction and polyoxotungstates clusters showing no trivalent metal are obtained as sodium salts (M^{III} = Co, Al, Ga); or (ii) the reaction takes place and the corresponding metal-substituted sandwich-type POM is obtained (M^{III} = Fe, Sc, Cr, Mn).

The first identification for all the solid products has been carried out on the basis of infrared spectroscopy. FT-IR spectroscopy has shown to be a simple, efficient and powerful tool for the identification of the obtained compounds prior to single-crystal X-ray diffraction experiments.

Two novel POMs have been isolated in the course of these studies namely the iron(acetate) trisubstituted Hervé-type $[\{Fe(C_2H_3O_2)\}_3(SbW_9O_{33})_2]^{12-}$ anion in **1-Fe** and the scandium substituted $[\{Sc^{III}(H_2O)_3\}\{WO_2(OH)\}(WO_2)_2(SbW_9O_{33})_2]^{10-}$ Krebs-type POM in **2-Sc**. In addition:

(a) Compound 1-Fe is the first example of an iron-substituted Hervé-type POM. Furthermore, it also constitutes the second example in the literature of a trivalent metal-substituted Hervé-type POM, suggesting that the formation of this kind of sandwich-type POM is not an exclusive feature of Mn^{III} cations.

(b) Compound **2-Sc** constitutes the second example of a scandium(III)-containing POM cluster. Scandium is expected to have the strongest Lewis acidity among rare earth metals, is compatible with water and Lewis bases, and is regarded as one of the standard and environmentally benign Lewis acids. All these advantages have led to an ever-growing attention for the enantioselective scandium-catalysed reactions.[51] The scandium metal centres in **2-Sc** have an appropriate disposition and three available coordination positions for the coordination of different substrates. All these facts make compound **2-Sc** a highly suitable candidate for catalytic applications, and

future studies will be carried out on both its optimized synthesis and potential catalytic properties.

(c) Compound **2-Mn** is a polymorph of an already published disubstituted Krebs-type POM with a different degree of hydration.

As for the employed characterisation techniques, (i) thermal and elemental analyses constitute the basic techniques for the chemical characterisation of newly synthesized POM clusters; (ii) single-crystal X-ray diffraction experiments are on the basis of the structural resolution of crystalline compounds; (iii) powder X-ray diffraction can be used for the identification of different crystalline phases in a given sample; and (iv) EPR spectroscopy can be used to determine the oxidation states and coordination environments of paramagnetic metal centres.

5. FUTURE WORK

In the course of these studies a new research line has been identified. The reaction of a great excess of an iron(III) salt with the Keggin-type $[B\text{-}\alpha\text{-}SbW_9O_{33}]^{9-}$ trilacunary anion in a sodium acetate buffered media has led to the isolation of red single-crystals that have been studied by FT-IR and single-crystal X-ray diffraction. The FT-IR spectrum of this compound and its comparison with the spectrum of compound **1-Fe** reported in this work (Figure 24) reveals the presence of a Hervé-type POM with acetate groups showing different coordination modes as can be observed by the multiple bands found in the organic region (> 1200 cm^{-1}).

The preliminary structural analysis shows an iron-trisubstituted Hervé-type $[Fe_3(SbW_9O_{33})_2]^{9-}$ POM with trinuclear acetate- and oxo-bridged $[Fe_3O(C_2O_2H_3)_6(H_2O)_3]^+$ iron(III) macrocations acting as counterions (Figure 25). The crystal packing of this compound shows structural voids, which may be interesting for different applications such as gas adsorption and storage, catalysis, etc.
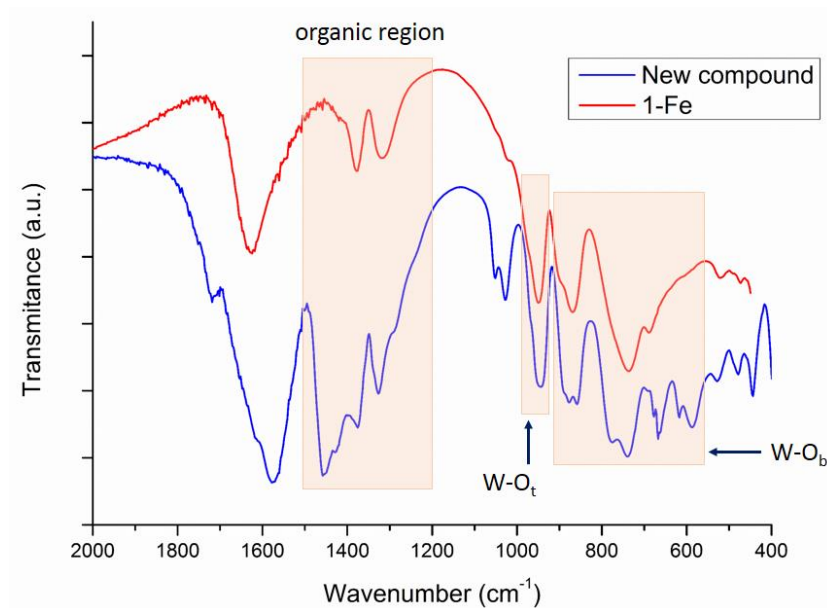
*Figure 24.- FT-IR spectra of the new compound together with that of **1-Fe**.*
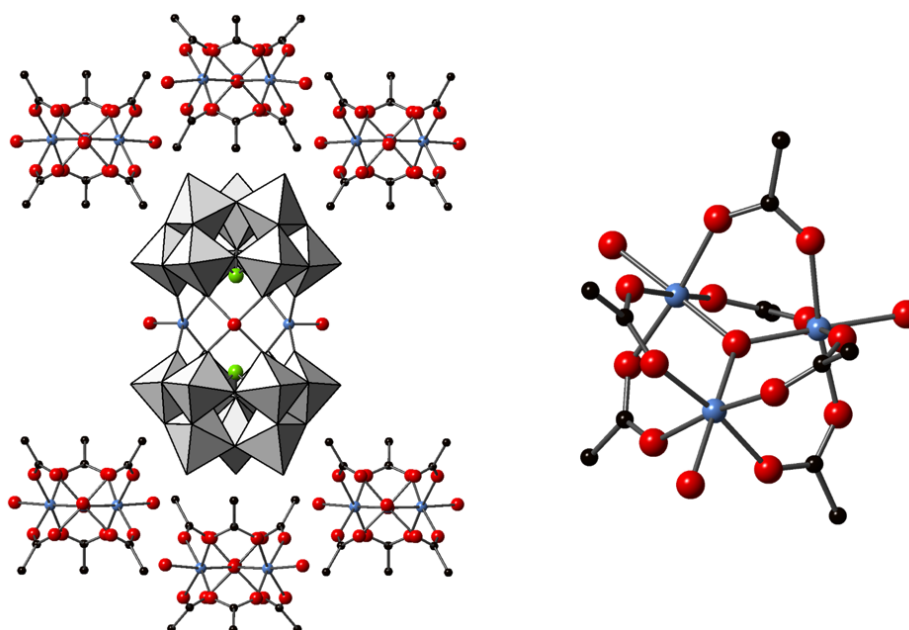

Figure 25.- Left: Distribution of the macrocations around the Hervé-type sandwich POM in the crystal structure of the new compound. Right: Detail of the trinuclear macrocation.

6. REFERENCES

1. Borrás-Almenar, J. J.; Coronado, E.; Müller, A.; Pope, M. T. *Polyoxometalate Molecular Science;* NATO Science Series; Kluwer: Dordrecht, The Netherlands, 2003.

2. Berzelius, J. J. *Poggend. Ann. Phys. Chem.* **1826**, *6*, 369-392.

3. De Luyart, F.; De Luyart, J. J. *Análisis Química del Volfram, y Examen de un Nuevo Metal, que Entra en su Composición;* Extractos de las Juntas Generales celebradas por la Real Sociedad Bascongada de Amigos del País: Vitoria, Spain, 1783; pp 46-88.

4. Keggin, J. F. *Nature* **1933**, *132*, 351.

5. Pope, M. T. *Heteropoly and Isopoly Oxometalates;* Springer-Verlag: Berlín, Germany, 1983.

6. Pope, M. T. In *Comprehensive Coordination Chemistry*; Wilkinson, G.; Gillard, R. D.; McCleverty, J. A., Eds.; Pergamon Press: New York, NY, USA, 1987; pp 1023-1058.

7. Sécheresse, F. *Polyoxometalate Chemistry: Some Recent Trends;* World Scientific: Singapore, 2013.

8. Nyman, M.; Bonhomme, F.; Alam, T. M.; Rodriguez, M. A.; Cherry, B. R.; Krumhansl, J. L.; Nenoff, T. M.; Sattler, A. M. *Science* **2002**, *297*, 996-998.

9. Lipscomb, W. N. *Inorg. Chem.* **1965**, *4*, 132-134.

10. Pope, M. T. *Polyoxometalates: From Platonic Solids to Anti-Retroviral Activity;* Topics in Molecular Organization and Engineering; Kluwer: Dordrecht, The Netherlands, 1994.

11. Baker, L. C. W.; Figgis, J. S. *J. Am. Chem. Soc.* **1970**, *92*, 3794-3797.

12. Casey, W. H. *Chem. Rev.* **2006**, *106*, 1-16.

13. Mialane, P.; Dolbecq, A.; Lisnard, L.; Mallard, A.; Marrot, J.; Sécheresse, F. *Angew. Chem. Int. Ed.* **2002**, *41*, 2398-2401.

14. Bösing, M.; Loose, I.; Pohlmann, H.; Krebs, B. *Chem. Eur. J.* **1997**, *3*, 1232-1237.

15. Oms, O.; Dolbecq, A.; Mialane, P. *Chem. Soc. Rev.* **2012**, *41*, 7497-7536.

16. Dolbecq, A.; Compain, J. -D.; Mialane, P.; Marrot, J.; Rivière, E.; Sécheresse, F. *Inorg. Chem.* **2008**, *47*, 3371-3378.

17. Evans, H.; Tourné, C.; Tourné, G.; Weakley, T. *J. Chem. Soc.* **1986**, 2699.

18. Knoth, W. H.; Domaille, P. J.; Harlow, R. L. *Inorg. Chem.* **1986**, *25*, 1577-1584.

19. Robert, F.; Leyrie, M.; Hervé, G. *Acta Crystallogr., Sect. B* **1982**, *38*, 358-362.

20. Bösing, M.; Nöh, A.; Loose, I.; Krebs, B. *J. Am. Chem. Soc.* **1998**, *120*, 7252-7259.

21. Kortz, U.; Nellutla, S.; Stowe, A. C.; Dalal, N. S.; Van Tol, J.; Bassil, B. S. *Inorg. Chem.* **2004**, *43*, 144-154.

22. Yamase, T.; Fukaya, K.; Nojiri, H.; Ohshima, Y. *Inorg. Chem.* **2006**, *45*, 7698-7704.

23. Kortz, U.; Al-Kassem, N. K.; Savelieff, M. G.; Al Kadi, N. A.; Sadakane, M. *Inorg. Chem.* **2001**, *40*, 4742-4749.

24. Mialane, P.; Marrot, J.; Rivière, E.; Nebout, J.; Hervé, G. *Inorg. Chem.* **2001**, *40*, 44-48.

25. Bi, L.; Reicke, M.; Kortz, U.; Keita, B.; Nadjo, L.; Clark, R. J. *Inorg. Chem.* **2004**, *43*, 3915-3920.

26. Drewes, D.; Piepenbrink, M.; Krebs, B. *J. Clust. Sci.* **2006**, *17*, 361-374.

27. Yamase, T.; Ishikawa, H.; Abe, H.; Fukaya, K.; Nojiri, H.; Takeuchi, H. *Inorg. Chem.* **2012**, *51*, 4606-4619.

28. Yamase, T. *J. Mater. Chem.* **2005**, *15*, 4773-4782.

29. Piepenbrink, M.; Limanski, E. M.; Krebs, B. *Z. Anorg. Allg. Chem.* **2002**, *628*, 1187-1191.

30. Artetxe, B.; Reinoso, S.; San Felices, L.; Vitoria, P.; Pache, A.; Martín-Caballero, J.; Gutiérrez-Zorrilla, J. M. *Inorg. Chem.* **2015**, *54*, 241-252.

31. Foster, K.; Bi, L.; McCormac, T. *Electrochim. Acta* **2008**, *54*, 868-875.

32. Bonchio, M.; Carraro, M.; Scorrano, G.; Kortz, U. *Adv. Synth. Catal.* **2005**, *347*, 1909-1912.

33. Carraro, M.; Bassil, B. S.; Soraru, A.; Berardi, S.; Suchopar, A.; Kortz, U.; Bonchio, M. *Chem. Commun.* **2013**, *49*, 7914-7916.

34. Artetxe, B.; Reinoso, S.; San Felices, L.; Lezama, L.; Gutiérrez-Zorrilla, J. M.; García, J. A.; Galán-Mascarós, J. R.; Haider, A.; Kortz, U.; Vicent, C. *Chem. Eur. J.* **2014**, *20*, 12144-12156.

35. Artetxe, B.; Reinoso, S.; San Felices, L.; Gutiérrez-Zorrilla, J. M.; García, J. A.; Haso, F.; Liu, T.; Vicent, C. *Chem. Eur. J.* **2015**, *21*, 7736-7745.

36. Artetxe, B.; Reinoso, S.; San Felices, L.; Lezama, L.; Gutiérrez-Zorrilla, J. M.; Vicent, C.; Haso, F.; Liu, T. *Chem. Eur. J.* **2016**, *22*, 4616-4625.

37. Artetxe, B. Systematic Studies on 3d- and 4f-Metal Containing Polyoxometalates Suitable for Organic Derivatization. Ph.D. Thesis, Universidad del País Vasco, UPV/EHU, Leioa, Spain, 2014.

38. Agilent Technologies UK Ltd. CrysAlisPro Software System, **2012**.

39. Dolomanov, O. V.; Bourhis, L. J.; Gildea, R. J.; Howard, A. K.; Puschmann, H. *J. Appl. Cryst.* **2009**, *42*, 339-341.

40. Sheldrick, G. M. *Acta Crystallogr., Sect. A: Found. Adv.* **2008**, *64*, 112-122.

41. Spek, A. L. *Acta Crystallogr., Sect. D: Biol. Crystallogr.* **2009**, *65*, 148-155.

42. Kortz, U.; Savelieff, M. G.; Bassil, B. S.; Keita, B.; Nadjo, L. *Inorg. Chem.* **2002**, *41*, 783-789.

43. FIZ Karlsuhe Inorganic Crystal Structure Database (ICSD). *https://icsd.fiz-karlsruhe.de* (accessed June 01, 2016).

44. Zhang, D.; Zhang, S.; Ma, P.; Wang, J.; Niu, J. *Inorg. Chem. Commun.* **2012**, *20*, 191-195.

45. Chrissafidou, A.; Fuchs, J.; Hartl, H.; Palm, R. *Z. Naturforsch., B: J. Chem. Sci.* **1995**, *50*, 217-222.

46. Nickolov, Z.; Georgiev, G.; Stoilova, D.; Ivanov, I. *J. Mol. Struct.* **1995**, *354*, 119-125.

47. Ma, X.; Song, K.; Cao, J.; Gong, P.; Li, H.; Chen, L.; Zhao, J. *Inorg. Chem. Commun.* **2015***, 60*, 65-70.

48. Wunderlich, B. Thermal Analysis Tools. In *Thermal Analysis of Polymeric Materials;* Springer-Verlag Berlin Heidelberg: The Netherlands, 2005; pp 428-429.

49. Murphy, D. M. EPR (Electron Paramagnetic Resonance) Spectroscopy of Polycrystalline Oxide Systems. In *Metal Oxide Catalysis*; Jackson, D., Hargreaves, J. S. J., Eds.; Wiley: Weinheim, Germany, 2009.

50. Carlin, R. L. *Magnetochemistry;* Springer-Verlag: Berlin, Germany, 1986; pp 328.

51. Pellissier, H. *Coord. Chem. Rev.* **2016***, 313*, 1-37.

7. ACKNOWLEDGEMENTS